val is 40 kg m^{-3} (*10*).
33. R. P. Turco *et al.*, *Icarus* **50**, 1 (1982).
34. See R. E. Arvidson *et al.* [*Science* **252**, 270 (1991)] for a more extensive description.
35. Retention ages for 20-km-sized craters on the North American and European cratons depend on erosion rate and lithology and vary from 34 to 630 Ma. Most craters larger than 20 km are recognizable to ages of 120 Ma, which gives a lower bound on retention age [R. A. F. Grieve], *Proc. Lunar Planet. Sci. Conf., Part 2, J. Geophys. Res.* **89**, B403 (1984).
36. The terrestrial data are from R. A. F. Grieve and M. R. Dence [*Icarus* **38**, 230 (1979)]; the lunar data are from R. Strom (personal communication).
37. G. A. Burba, *Lunar Planet. Sci.* **XX**, 123 (1989).
38. J. J. Plaut and R. E. Arvidson, *J. Geophys. Res.* **93**, 15,339 (1988).
39. G. G. Schaber, *U.S. Geol. Surv. Open-File Rep. 90-468* (1990).
40. W. Feller, *An Introduction to Probability Theory and Its Applications* (Wiley, New York, 1962).
41. Image mosaics for the Sappho region were not available when this paper was prepared, so no geological assessment has been made.
42. R. E. Grimm and S. C. Solomon, *J. Geophys. Res.* **93**, 11,911 (1988).
43. Mean oceanic crustal thickness of 6 km multiplied by plate creation rate of 3 km^2 yr^{-1} [B. Parsons, *Geophys. J. R. Astron. Soc.* **67**, 437 (1981); A. Reymer and G. Schubert, *Tectonics* **3**, 63 (1984)].
44. R. E. Grimm and S. C. Solomon, *Geophys. Res. Lett.* **14**, 538 (1987).
45. R. E. Arvidson *et al.*, *ibid.* **17**, 1385 (1990).
46. This result can be derived as follows: Consider that the resurfacing rate is linear in time and that the time to resurface the planet once is given by T_r. Then there is a complete spectrum of production ages ranging from the present back to T_r, and all ages are equally likely to be found on the planet. For any given age, t, within this spectrum, the total number of craters found on the planet is given by

$$\Sigma_r(D,t) = R_p t D^{-\alpha}\, da$$

where da is the incremental surface area of the planet of production age t. The total number of craters on the planet can then be obtained by integrating over the surface area of the planet. Equivalently, if f_r is the fractional resurfacing rate (fraction of planet resurfaced per unit time), then da is related to incremental time dt by $da = Af_r dt$. Then the total number of craters may also be obtained by integrating over all possible production ages

$$\Sigma_r(D) = D^{-\alpha} \int_0^{T_r} R_p t A f_r dt$$

$$= R_p \frac{T_r^2}{2} A f_r D^{-\alpha}$$

Cumulative size-frequency density is obtained by dividing by planetary surface area, and noting that T_r must be the reciprocal of f_r, we then find that

$$\Sigma_r(D) = \frac{1}{2} \frac{R_p}{f_r} D^{-\alpha}$$

47. Estimates of R_p and α are based on the production rate of craters >20 km in diameter by Venus-crossing asteroids, not including asteroids of cometary origin or active comets (E. M. Shoemaker and C. S. Shoemaker, in *The New Solar System*, J. K. Beatty and A. Chaikin, Eds. (Sky Publishing, Cambridge, MA, 1990), pp. 259–274.
48. This work was supported in part by various Magellan contracts from the Jet Propulsion Laboratory, California Institute of Technology, to the authors' home institutions, and by a grant from NERC to J.E.G. at the University of London Observatory. R.J.P. was also supported by NASA grant NAGW-459 to Southern Methodist University. We would like to thank R.E. Grimm, R. R. Herrick, M. Ravine, P. Schenk, V. L. Sharpton, N. Stacy, and C. Wiles. S. Yewell helped provide the photographic products for this paper. Useful comments on the original manuscript were supplied by H. J. Melosh, and R. A. F. Grieve and P. H. Schultz provided detailed reviews. We gratefully acknowledge the Magellan teams at JPL and Martin Marietta who made all of this possible.

8 January 1991; accepted 18 March 1991

Venus Tectonics: Initial Analysis from Magellan

SEAN C. SOLOMON, JAMES W. HEAD, WILLIAM M. KAULA, DAN MCKENZIE, BARRY PARSONS, ROGER J. PHILLIPS, GERALD SCHUBERT, MANIK TALWANI

Radar imaging and altimetry data from the Magellan mission have revealed a diversity of deformational features at a variety of spatial scales on the Venus surface. The plains record a superposition of different episodes of deformation and volcanism; strain is both areally distributed and concentrated into zones of extension and shortening. The common coherence of strain patterns over hundreds of kilometers implies that many features in the plains reflect a crustal response to mantle dynamic processes. Ridge belts and mountain belts represent successive degrees of lithospheric shortening and crustal thickening; the mountain belts also show widespread evidence for extension and collapse both during and following crustal compression. Venus displays two geometrical patterns of concentrated lithospheric extension: quasi-circular coronae and broad rises with linear rift zones; both are sites of significant volcanism. No long, large-offset strike-slip faults have been observed, although limited local horizontal shear is accommodated across many zones of crustal shortening. In general, tectonic features on Venus are unlike those in Earth's oceanic regions in that strain typically is distributed across broad zones that are one to a few hundred kilometers wide, and separated by stronger and less deformed blocks hundreds of kilometers in width, as in actively deforming continental regions on Earth.

IT HAS BEEN KNOWN FOR MORE THAN A decade that the Venus surface preserves a rich and complex history of deformation of the lithosphere, the layer of long-term strength that constitutes the outer shell of every terrestrial planet. The Pioneer Venus altimeter revealed the presence on Venus of such large-scale tectonic structures as great rift zones and linear mountain belts (*1–3*). Radar images of the surface obtained by the Venera 15–16 orbiters (*4, 5*) and Earth-based radar observatories (*6–10*) have shown a variety of features interpreted to be of tectonic origin. The radar images from Magellan constitute an improvement in resolution by at least an order of magnitude over the best images previously available (*11*). In this paper, we discuss what those images, and their interpretations, are revealing about the styles of lithospheric deformation on Venus, the inferred mechanical properties of the lithosphere, and their implications for the tectonic history of the planet. We restrict the discussion principally to data obtained during the first month of mapping, representing about 15% of the surface of the planet.

S. C. Solomon, Department of Earth, Atmospheric, and Planetary Sciences, Massachusetts Institute of Technology, Cambridge, MA 02139.
J. W. Head, Department of Geological Sciences, Brown University, Providence, RI 02912.
W. M. Kaula and G. Schubert, Department of Earth and Space Sciences, University of California, Los Angeles, CA 90024.
D. McKenzie, Bullard Laboratories, Cambridge University, Cambridge CB3 OEZ, England.
B. Parsons, Department of Earth Sciences, Oxford University, Oxford OX1 3PR, England.
R. J. Phillips, Department of Geological Sciences, Southern Methodist University, Dallas, TX 75275.
M. Talwani, Houston Area Research Center, The Woodlands, TX 77381.

Plains deformation. The plains, which constitute more than 80% of the surface of Venus (*2*), are generally low-relief areas with surface deposits of volcanic origin (*12, 13*). Although a few plains regions viewed by Magellan to date are nearly devoid of tectonic features, most show considerable evidence for deformation in a variety of forms and patterns (*11*) that in some areas are consistent over distances of hundreds of kilometers. Because of the generally limited magnitude of horizontal strain in most plains regions, the sense of strain and its relation to regional topography can be more evident in the plains than in areas of greater relief and more intensive deformation.

One of the regions of more extensively deformed plains is centered near 32°N, 335°E, between Guinevere and Sedna Planitiae. [A global map of named features is in (*11*)]. Throughout an area of about 10,000 km^2, these plains are marked by hundreds of prominent lineations trending approximately NW. In one part of this region (Fig. 1) the lineations are paired normal faults bounding flat-floored depressions spaced 0.5 to 3 km apart. These features are interpreted to be simple graben, the result of limited horizontal stretching of the upper crust in the NE-SW direction. A few bright, irregular depressions trending WNW to E-W appear to consist of coalesced sections of NW-trending graben and may represent a younger episode of more nearly N-S extension.

The plains record a continuing interplay between deformation and volcanism. For example, in another area (Fig. 2) approximately 150 km to the SE of that shown in

Fig. 1. A Magellan radar image of a section of lineated plains 10,000 km^2 in area located between Guinevere and Sedna Planitiae and centered at 30°N, 335°E. In this image, located at 33°N, 331°E, and 140 km wide, most of the linear features are walls of flat-floored graben trending approximately NW and spaced at 0.5 to 3 km. North is up in this image and in all images to follow.

Fig. 1 the NE-trending lineations are mantled by small volcanic pits and domes and their associated deposits. A few of the domes appear to be cut by lineations; these relations indicate that faulting both postdates and predates the volcanic activity. A broad rise or saddle, several hundred meters in relief, separates Sedna Planitia to the north from Guinevere Planitia to the south and occupies a part of an area of apparently disrupted plains previously identified from Arecibo images as linking Beta Regio to the west and Eistla Regio to the east (*14*). The concentration of most intense plains deformation and volcanic resurfacing (Figs. 1 and 2) in the vicinity of the crest of this rise and the persistence of the deformational patterns over hundreds of kilometers suggest that the region may have been thermally uplifted and stretched as a result of convective upwelling of the underlying mantle.

A remarkably regular and nearly orthogonal pattern of crosscutting lineations is observed (Fig. 3) 100 to 300 km to the southeast of the region shown in Fig. 2. There are two sets of lineations: a brighter set trending NW and a fainter set trending NE. The fainter lineations have a very regular spacing of about 1.2 km; many individual lineations are continuous for several tens of kilometers. The brighter lineations are for the most part less continuous and have an approximate spacing of 2 to 3 km. Some, however, continue for distances of several hundred kilometers; two examples of these longer lineations, spaced 45 km apart, can be seen in Fig. 3. Because the brighter lineations are parallel or even colinear with features to the northwest interpreted to be graben (Figs. 1 and 2), we infer that these lineations are also normal faults produced by limited NE-SW extension.

The regular spacing of the fainter set of lineations may result from deformation of a surface layer whose thickness is nearly uniform and which was acted upon by a principal normal stress that was oriented perpendicular to the lineation direction and that varied only slightly over the region. Although different mechanisms, such as necking or buckling of an elastic layer over a viscous medium (*15*) or deformation of a plastic or viscous layered structure (*16*), give somewhat different results for the characteristic wavelength λ of deformation that would be expected to develop, a reasonable rule of thumb is that $2\pi d/\lambda \approx 1$, where d is the layer thickness. This relation gives a layer thickness of about 200 m for this region. If the physical properties of diabase are appropriate to the Venus crust, then one would expect the strong upper crustal layer to have a thickness of 2 to 4 km when in thermal equilibrium with a temperature gradient of 15 K/km (*16*), too thick to constitute the layer that deformed to yield the pattern seen in Fig. 3. If this plains surface formed as a thick deposit of completely molten lava, it would take only 600 years of cooling for a solid layer 200 m thick to develop at the surface (*17*). One possibility, therefore, is that we are looking at the deformation of a thin, near-surface layer once underlain by molten or nearly molten and highly ductile material. The nearly right angle at which the two sets of lineations intersect might be the result of a temporal switch in the relative magnitudes of two horizontal extensional principal stresses.

Although the pattern of crosscutting lineations is striking, it is observed only over a relatively small part of the plains imaged by Magellan in the first month of mapping. Elsewhere in the plains, complex and irregular patterns of radar-bright lineations (Fig. 4) are observed. The length scales of the patterns are similar to the spacing of the faint lineations in the cross-cutting pattern in Fig. 3. The lineations are also commonly associated with small volcanoes and their deposits (Fig. 4). These characteristics suggest that such irregular patterns may also result from deformation of a thin surficial

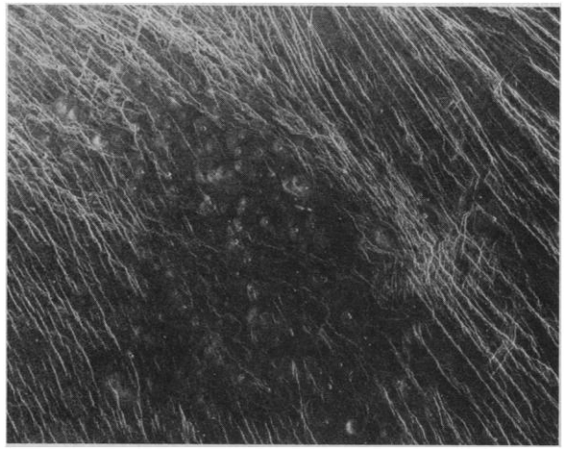

Fig. 2. In this Magellan radar image the NW-trending lineations are partially mantled by volcanic deposits. The image, 140 km wide, is centered at 32°N, 332°E, southeast of the area in Fig. 1. The small volcanic pits, domes, and associated deposits and the faulting of some of the domes illustrate the continuing interplay between deformation and volcanism in these plains.

Fig. 3. A Magellan radar image of two nearly orthogonal sets of lineations. The image is centered at 30°N, 333°E, south of the area in Fig. 2, and is 75 km wide. There is no more than about 100 m of relief over the region shown; the downhill direction is approximately to the SE (see text).

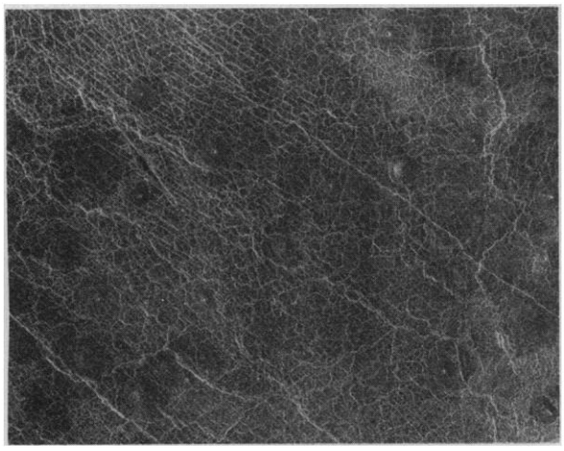

Fig. 4. This image depicts another type of small-scale tectonic pattern located farther south in the plains at 22°N, 334°E. Although the pattern is more complex in this region, a NW trend is still the most prominent. Small volcanoes and their deposits both cut and are cut by the lineations. The image is 110 km wide.

layer shortly after volcanic resurfacing, but in situations where the properties of the layer or of the forces acting on it were not uniform in space or time.

Another type of deformational feature common in the plains are linear, regularly spaced ridges (see below for examples). In morphology and spacing these features appear similar to wrinkle ridges in lunar maria and martian ridged plains and attributed to modest levels of horizontal compression and shortening (*18*).

Ridge and groove belts. Deformation in a number of lowland regions on Venus is concentrated into distinct linear zones or belts (*5, 9*). These deformation belts are generally elevated by several hundred meters above the surrounding plains and contain curvilinear, commonly anastomosing concentrations of subparallel ridges and grooves trending approximately parallel to the margins of the belts. The ridges and grooves can be continuous for hundreds of kilometers. In Venera 15–16 and Arecibo images of deformation belts, the ridges or grooves appear to be spaced 10 to 20 km apart. Deformation belts in the area of Venera 15–16 coverage have been generally interpreted to be compressional features, on the basis of their morphology and positive relief (*5, 19, 20*), but an extensional origin also has been suggested (*21*).

Lavinia Planitia, a broad lowland centered at about 50°S, 340°E, is known from Arecibo images to contain a number of deformation belts (*9*). Magellan images provide the first high-resolution views of these features. The belts in this region (Fig. 5) are elevated, radar-bright, intensely deformed curvilinear regions separated by generally darker, smoother, and lower plains. The generally positive relief of the belts supports the hypothesis that they are products of lithospheric shortening and crustal thickening. Radar brightness, perhaps indicative of intensity of deformation, correlates approximately with total relief, presumably a measure of crustal shortening.

The Lavinia belts display a wide range of small-scale morphology. One of the simplest belt segments (Fig. 6) is characterized by broad, NW trending arches that vary considerably in width, both from one to the next and along a single arch; the maximum width is about 9 km. The broadest arches appear markedly asymmetric and have a narrow, rugged secondary ridge superimposed on their SW flank. Some narrow ridge segments occur without any underlying arch. Typical widths for the smaller ridges are 2 km. The ridges and arches in this area bear a number of similarities to lunar mare ridges and arches, including morphology, planform, and dimensions, and by analogy they are interpreted as compressional tectonic structures (*18*). This ridge belt formed as a result of a greatest compressive stress that was oriented NE-SW.

We have selected two deformation belts in the Lavinia Planitia region for detailed analysis. The first is a feature named Hippolyta Linea, a belt 150 to 200 km wide centered near 41°S, 342°E, and trending WNW (Fig. 7A). Most of the belt is distinctly elevated above the surrounding plains; typical relief

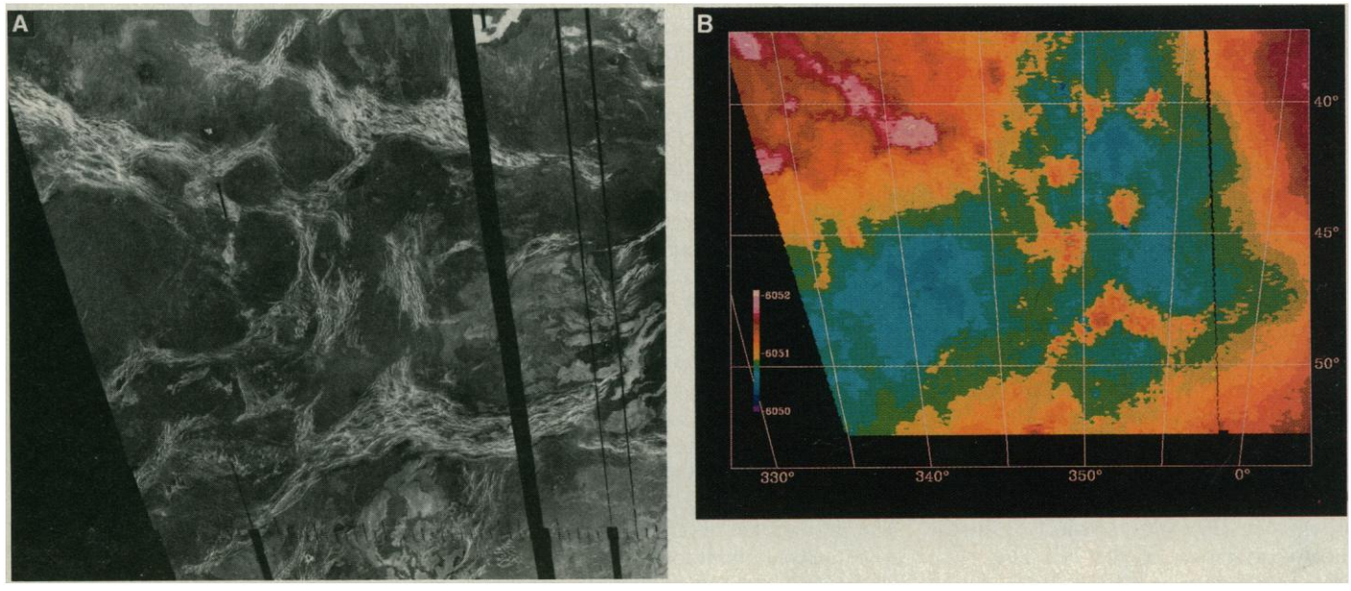

Fig. 5. (**A**) Magellan radar image of ridge and groove belts in Lavinia Planitia. Each belt consists of one or more broad ridges with superposed narrower tectonic lineations. Along those ridges trending WNW these lineations are graben or narrow fractures spaced 1 to 10 km apart; along those trending NE the lineations consist of narrower ridges about 5 km wide and 5 to 15 km apart. The image is centered at 350°E, 45°S, and is 1850 km wide at the top. (**B**) Color-contoured Magellan altimetry of the same region; contours are planetary radius in kilometers. (The altimetry coverage extends to the west of the imaging coverage.) The belts are seen to stand several hundred meters above the surrounding plains.

Fig. 6. Magellan radar image of a simple ridge belt showing morphology similar to that of lunar mare ridges and arches. The belt extends northwestward into an area not yet imaged by Magellan. The image is centered at 36°S, 338°E, and is 40 km wide at the top.

is 500 m and the maximum relief approaches 1 km (Fig. 7B). A few broad arch-like ridges with widths of 3 to 5 km are present, mostly along the northern margin of the belt. The bulk of the belt, however, is dominated by a complex array of linear to arcuate faults and fractures, some paired to form grooves with typical widths of 1 to 2.5 km. There are two dominant fault strikes within the belt: WNW, aligned approximately with the margins of the belt, and NW. Many faults change intermittently along strike, in some cases abruptly, from one of these trends to the other. In general, faults aligned NW appear to have greater displacements than those aligned WNW. When individual faults, especially paired ones, switch from the WNW trend to NW, their offsets typically increase in magnitude; this increase results in several areas of topographically depressed, rhombohedrally shaped blocks (Fig. 7C). Such features may be the result of a modest component of right-lateral shear accompanying groove formation.

In some parts of the belt faults are densely and fairly regularly spaced, typically a few hundred meters apart. In other parts, however, two distinct scales of fault spacing are evident (Fig. 7, A and C). Faults are concentrated into bands of intense deformation that are associated generally with the highest topography (Fig. 7B), particularly in the south-central part of the belt (Fig. 7C) where the bands are spaced 20 to 30 km apart. This spacing is consistent with deformation of the entire thickness of the strong upper crustal layer (*16*); the finer spacing between individual lineations, by this hypothesis, represents internal deformation of blocks of upper crust. There is not always a simple one-to-one correspondence between deformation and elevation, however; for example, the zone of straight WNW-trending faults in the southeastern corner of Fig. 7A lies at essentially the same elevation as the surrounding plains (Fig. 5B).

In contrast to some of the other belts in Lavinia Planitia, Hippolyta Linea contains evidence for volcanism within the belt. Volcanism is displayed best in a broad region in the west-central portion of the belt, centered around 40.5°S, 340°E (Fig. 7, A and D). The terrain here is smooth and radar-dark, faulting is minor, and ridges are absent. Volcanic material is ponded in low-lying regions. Within the dark material are abundant small pits with diameters up to 1 km. A few small, irregular domes are also present.

Much of the faulting in Hippolyta Linea, and in other groove belts in Lavinia Planitia, appears extensional in character, marked by numerous narrow, shallow graben. The concentration of extensional faulting along the crests of topographic highs, however, may indicate that the extension is a local effect of flexure across the crests of broad anticlines (*22*). This phenomenon is observed on Earth in regions where folding is recent or rapid with respect to erosion rates, so that the uneroded uppermost surface of the folded unit is preserved. A variety of other types of faulting and fracturing is found in association with folding as well, ranging from tension fractures to deep-seated thrust faults that can splay to complex geometries as they approach the surface (*22*). Faulting of all of these types may be significant in Hippolyta Linea. Where extensional faulting in the belts is not concentrated along the crests of broad ridges, an argument for its link to regional compression is more difficult to make. In these areas, the primary argument for a compressional origin for the belt is simply its elevated topography.

The second deformation belt, located about 800 km south of Hippolyta Linea, is 35 to 40 km wide and is composed of a number of subparallel ridges, many arch-like in profile (Fig. 8). Ridge widths range from more than 5 km to less than 1 km. Ridges are sinuous and commonly bifurcate and merge in complex anastomosing patterns. This belt is transected by two sets of tectonic lineations (Fig. 8B). One set, trending NW, consists of a number of straight grooves. The grooves are about 500 m wide, and some are continuous for more than 100 km. The second set of lineations is substantially less regular and is most prominent in the south-central part of the region. Rather than long grooves, this set consists of shorter, less regular radar-bright lineations with widths near the resolution limit and no clear topographic expression. They may be grooves with widths too small to be resolved. These second lineations display a distinct change in trend within the ridge belt. They have a WNW trend to the east and west of the belt but a ENE trend within the belt.

Crosscutting relations show that, with only one or two possible exceptions, lineations of the first set postdate formation of the ridge belt. The lineations of the second set, however, are commonly (although not always) crosscut by the ridges and appear for the most part to predate them. In the relatively few cases where lineations of the second set cut across ridges they may still predate them; if the ridges formed by low-amplitude folding, their formation would not necessarily have completely disrupted preexisting fractures.

As seen here and elsewhere on Venus, long, narrow, straight lineations are common. The change in trend of the older lineations as they enter and leave the ridge belt suggests that they, too, may have originally been straight but were deformed in the same episode that produced the belt. The lineations enter the belt from the SE at an angle that is about 20° to 25° from normal to the belt axis. Within the belt this angle increases, consistent in principle with deformation by shortening across the belt. If the observed changes in trend of the lineations resulted purely from deformation of straight lineations by compression oriented perpendicular to the belt axis, a compressional strain of 20 to 30% across the belt would be implied. Alternatively, the compression that formed the belt may have been accompanied by some left-lateral shear distributed across the belt. Required shear strains in this case (calculated for simple shear along the direction of the belt axis) would not exceed 10 to 20%. Although there is no independent evidence that the older lineations in the region of this image were initially straight, similar lineations are bent or offset, also in a left-lateral sense, by other NE-trending ridge belts in the Lavinia Planitia area. These relations support the hypothesis that shear often accompanies shortening in ridge belt deformation.

On a large scale the various belts show several significant regional trends (Fig. 5). The ridge belts, consisting of simple subparallel ridges, are generally oriented NE-SW to NNE-SSW (Fig. 8). In contrast, the groove belts like Hippolyta Linea that are expressed morphologically primarily by small-scale extensional features are mostly oriented E-W to WNW. These regional trends are also reflected in small-scale tectonic features on the plains separating the belts. Most of the ridge belts are aligned parallel to

low, arcuate or sinuous ridges on the surrounding plains. Some of the ridges in the belts even merge with these features. The groove belts, on the other hand, lie parallel to and commonly merge with groove-like lineations of the sort observed crosscutting the ridge belt in Fig. 8. Finally, as shown in Fig. 5B, the groove belts consistently rise to higher maximum elevations than do the ridge belts.

Overall, the deformation belts in Lavinia Planitia appear to result primarily from modest amounts of compression and crustal shortening across the belts, coupled in some cases with distributed shear. The differing morphological expression of shortening, however, may reflect some basic differences in their formation mechanism. Ridge belts appear to result from buckling or fault-bend folding of a competent surface layer. Groove belts, on the other hand, exhibit evidence for extension of a shallow layer that may result from fracturing of the lithosphere as it is stretched across a broad uplift. Some of the differences in small-scale morphology could be due to a superposed regional stress field in which the greatest and least compressive horizontal stresses are oriented approximately WNW-ESE and NNE-WSW, respectively. In general, the concentration of most of the deformation in Lavinia Planitia into distinct belts, with the intervening blocks remaining comparatively undeformed, is reminiscent of some zones of intracontinental deformation on Earth. In particular, the pattern of compression and shear accommodating lithospheric shortening in northeastern Iran (*23*) is similar in spatial scale and distribution and in topographic relief to that shown in Lavinia Planitia. Achieving a quantitative understanding of that similarity for regions of two planets with different interior thermal structures and presumably different crustal structures should offer a better understanding of the mechanical properties of the lithosphere on both planets.

Mountain belts. The greatest deformation on Venus is seen in the mountain belts, which reach elevations in excess of 10 km above mean planetary radius (*1*). The only known mountain belts on Venus are the

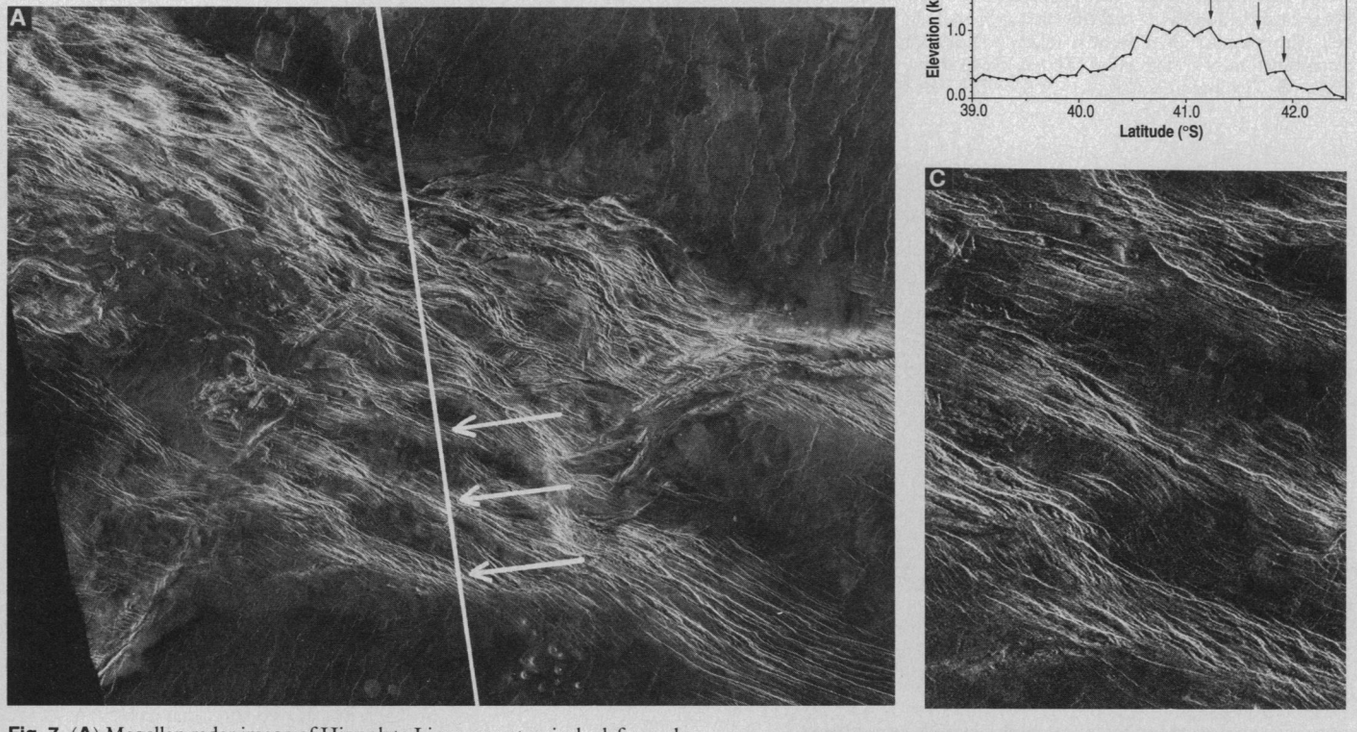

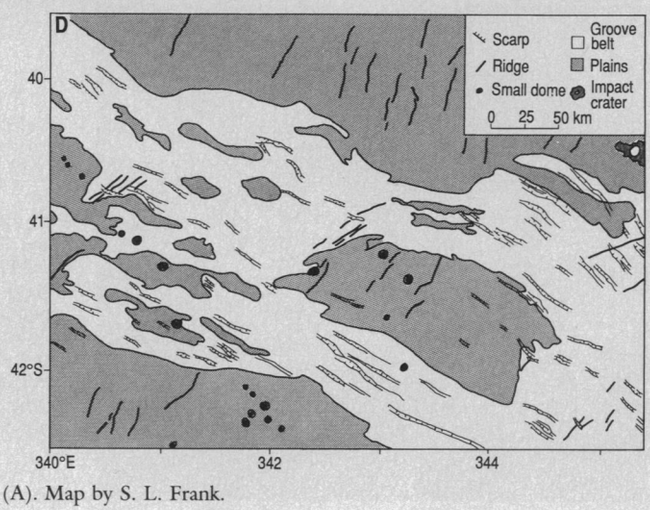

Fig. 7. (**A**) Magellan radar image of Hippolyta Linea, an extensively deformed belt lying up to 700 m above the surrounding plains. In the plains, sinuous ridges are similar in scale, morphology, and spacing to wrinkle ridges on the moon, Mars, and Mercury (*18*). Most of the ridges in this image trend NE to NNE, although a few trend NNW. The spacing of the NE-trending ridges is approximately 20 km; this spacing is consistent with deformation of the entire thickness of the strong upper crustal layer (*16*). The image is centered near 41°S, 342°E, and is 430 km wide. (**B**) Profile of altimetry along the track shown in (A); arrows correspond to those in (A); 1° latitude equals 105.6 km on Venus. All of Hippolyta Linea is seen to be elevated with respect to the surrounding plains, and the individual concentrations of grooves (arrows) are also 50 to 100 m higher than the less deformed regions of plains between them. The correlation between high topography and intensity of deformation suggests that the belt and associated deformational features formed by crustal shortening. The presence of NE-trending sinuous ridges within less deformed but elevated portions of Hippolyta Linea indicates that the plains deformation that produced these ridges predated formation of the groove belt. (**C**) Detail of the lower central portion of (A), showing that the individual small-scale tectonic features consist primarily of WNW-trending scarps, some arranged in horst-and-graben structures. The scarps in this image, 85 km in width, are concentrated into bands 10 to 20 km wide. (**D**) Geological sketch map of Hippolyta Linea; the map boundaries differ slightly from those of the image in (A). Map by S. L. Frank.

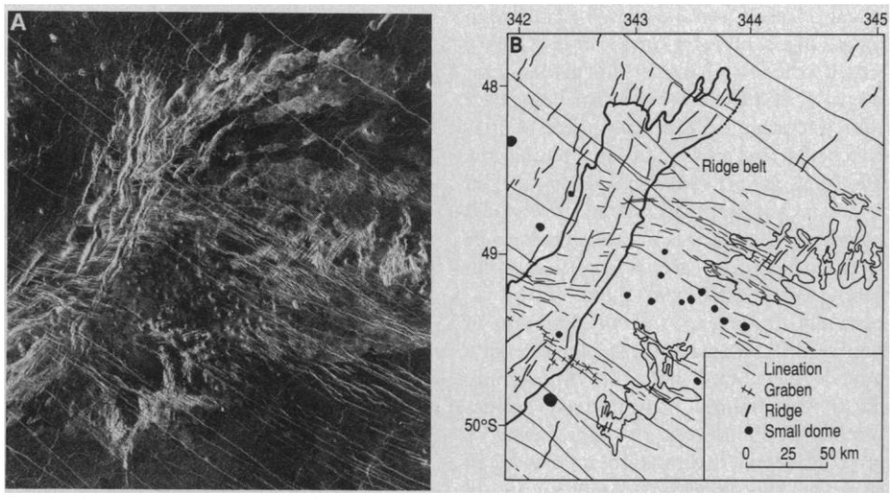

Fig. 8. (**A**) Magellan radar image of a ridge belt transected by two sets of tectonic lineations. This belt rises 200 m above the surrounding plains and consists of NE-trending ridges 1 to 5 km wide, spaced 5 to 15 km apart. Long, narrow lineations, some of which are graben, trend primarily E-W to NW. Some of these lineations curve as they approach, and appear to be offset horizontally across, the ridge belt. The combination of positive relief and horizontal offset suggests that this ridge belt was formed by a combination of compression and left-lateral shear. The image, centered near 49°S, 343°E, is 240 km wide. (**B**) Geological sketch map of the ridge belt by S. L. Frank.

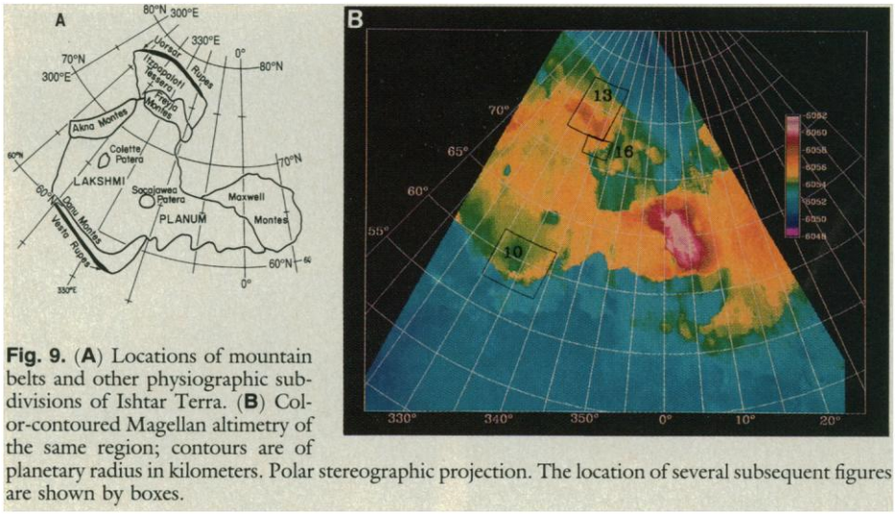

Fig. 9. (**A**) Locations of mountain belts and other physiographic subdivisions of Ishtar Terra. (**B**) Color-contoured Magellan altimetry of the same region; contours are of planetary radius in kilometers. Polar stereographic projection. The location of several subsequent figures are shown by boxes.

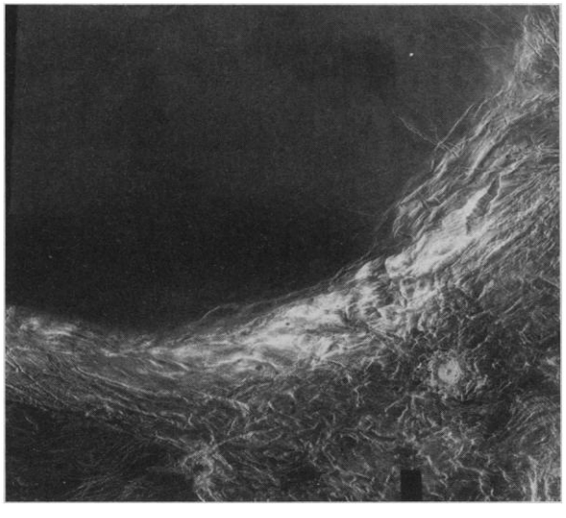

Fig. 10. Magellan radar image of Danu Montes and southern Lakshmi Planum. The brightest areas correspond approximately to the topographic highs along Danu Montes, which rise up to 2 km above Lakshmi Planum to the north and drop steeply by 2 to 4 km to the plains to the south. The prominent impact crater at 58.6°N, 337°E, is Magnani. This image is centered near 59°N, 335°E, and is 550 km wide at the base.

four surrounding Lakshmi Planum in Ishtar Terra: Akna, Danu, Freyja, and Maxwell Montes (Fig. 9). Of these belts, Danu Montes and large portions of Freyja Montes have been imaged by Magellan in the first month of mapping.

On the basis of topography and morphology as seen in Venera 15–16 and Arecibo images, the mountain belts have been inferred to be zones of lithospheric compression and crustal shortening and thickening (*5, 24*). From topographic profiles, it has been suggested that some of this shortening has been accomplished by underthrusting and flexure of the lithosphere at the edges of several of the belts (*25, 26*). One hypothesis is that the formation of the mountain belts was driven by shear tractions at the base of the lithosphere associated with a cylindrical center of downwelling mantle flow beneath Ishtar Terra (*27, 28*). Two other aspects of Ishtar Terra, however, have been invoked in support of an alternative hypothesis. First, Lakshmi Planum, surrounded on nearly all sides by mountain belts, is the site of significant plains volcanism and two major volcanic edifices: Colette and Sacajawea Paterae (*12, 13, 29*). Second, from gravity-anomaly modeling, the long-wavelength topography has an apparent depth of compensation of 130 km, too great to be due to crustal thickness variations and difficult to reconcile with simple mantle downwelling models (*30*). These considerations led to the hypothesis that Lakshmi Planum overlies a region of cylindrical mantle upwelling and that the mountain belts have formed over regions of downward return flow (*31*) where strain has perhaps been localized by a horizontal discontinuity in lithospheric strength between the thermally weakened plateau and the surrounding regions (*30*).

Danu Montes extend for more than 1200 km along the southern and southeastern edge of Lakshmi Planum (Fig. 10) and rise up to 3 km above the adjacent plains (Fig. 9B). To the south of the western arm of Danu Montes the elevation drops steeply along Vesta Rupes (Fig. 11), a narrow scarp the base of which is 2.5 km or more below Lakshmi Planum. Magellan altimetry indicates that, for a significant length of Vesta Rupes, much or all of this elevation change takes place between two successive altimeter samples (spaced about 7 km apart at this latitude); thus the scarp must have an average slope in excess of 20° over this horizontal distance. The topographic relief of the mountain belt is greatest along the northeastern arm; the highest areas correspond approximately to the bright areas in the radar image in Fig. 10, indicating high surface roughness and high rms slope. We interpret the trend of the topography as

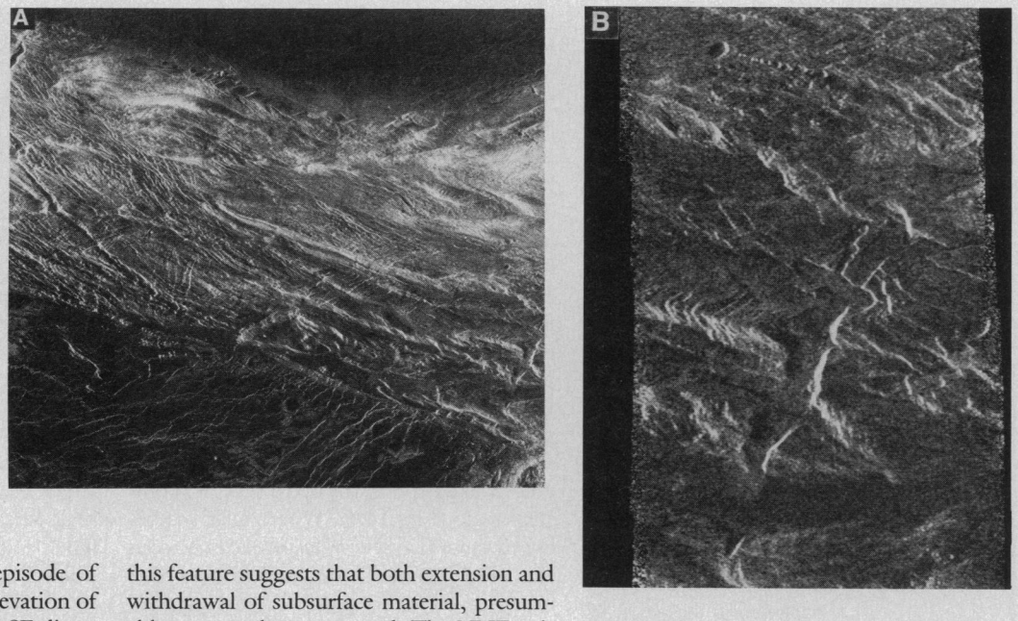

Fig. 11. (**A**) An expanded view of a part of Fig. 10 along the western arm of Danu Montes and the steep slope to the plains to the south. The bright areas are of high roughness and high rms slope. This image is centered near 58°N, 331°E, and is 190 km wide at the base. NW-striking normal faults and graben run subparallel to obliquely to the topographic contours and are generally consistent with downslope extension of the upper crustal layer. Fainter lineations, at least some of which are troughs, trend to the NE. (**B**) Detailed view of the eastern edge of (A). From the southern edge of the image to the crest of Danu Montes near the northern edge there is an increase in elevation of 2.5 km. The image is 30 km wide.

indicating that the most recent episode of compression responsible for the elevation of this mountain belt was in the NW-SE direction. A number of thrust systems are evident as plateau-facing scarps where the mountain terrain steps up from Lakshmi Planum, particularly along the northeastern arm of the mountain belt (Fig. 12). The development of thrust faults and wrinkle ridges parallel to the trend of the topography in the plains of Lakshmi Planum adjacent to the northeastern arm of Danu Montes and the upward tilt of the plains toward the mountain belt (Fig. 9B) suggest that the nearby plains were involved in the crustal shortening that accompanied mountain formation.

Magellan images also reveal widespread evidence for extension of the upper crust of both Danu Montes and Vesta Rupes. In Fig. 11, numerous NW-striking normal faults and graben run subparallel to oblique to the trend of Vesta Rupes. Fainter lineations, at least some of which are troughs, trend NE. The spacing between adjacent extensional features, 1 to 5 km, indicates that the deformation is primarily of the upper crust rather than the lithosphere as a whole. Several important relations are evident along the steep slope south of the crest of Danu Montes near the junction between the two arms of the mountain belt (Fig. 11B). Here, the dominant tectonic grain trends WNW, approximately parallel to the inferred direction of most recent compression. Two collapse features suggest that magmatism accompanied extension of the upper crust. The first of these is a chain of partially coalesced pits aligned with the WNW trend (Fig. 11B, top). The second (Fig. 11B, center) is the relatively young, irregularly shaped, flat-floored depression running perpendicular to the regional tectonic trend; the combination of curved and straight segments making up the outline of this feature suggests that both extension and withdrawal of subsurface material, presumably magma, have occurred. The NNE orientation of this feature is somewhat of an anomaly and is perhaps related to its location on the slope outward of the bend in the mountain belt.

Along the northeastern arm of Danu Montes (Fig. 12) are a number of partially coalesced pits, graben, and collapsed troughs trending NW to E-W and crossing the thrust systems. Some of the collapse features grade downslope into sinuous depressions and indicate withdrawal and channeling of magma toward the plains of Lakshmi Planum. Most of these features appear to cut the thrust faults they transect; the implied magmatism apparently occurred more recently than much of the mountain building.

The numerous extensional features along Danu Montes and Vesta Rupes probably have several causes. The predominance of approximately NW-trending extensional structures (Figs. 10 to 12) and the inferred NW-SE direction for the most recent episode of compression suggest that lateral extension of the crust in the NE-SW direction has accompanied crustal shortening. Such a phenomenon is seen in terrestrial mountain belts, such as the Himalaya (*32*), and is the natural consequence of the tendency of thickened and elevated crust to spread under the influence of gravity. During periods of ongoing convergence, the free direction for such extension is orthogonal to the direction of shortening. The extensional structures in the vicinity of Vesta Rupes may be the result of gravity sliding of

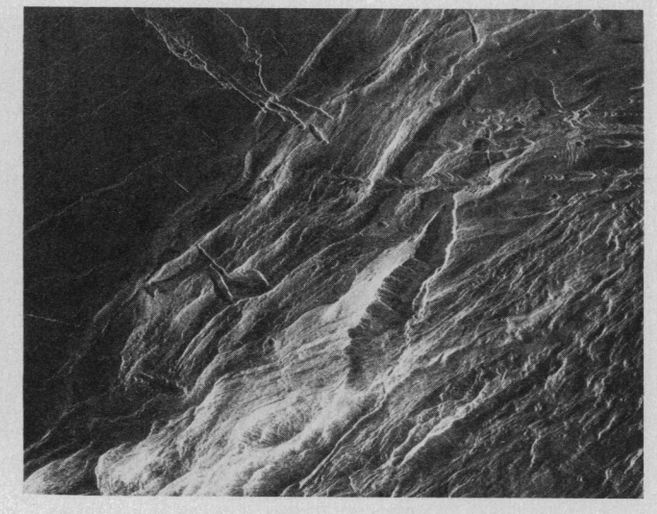

Fig. 12. Magellan radar image of the crest of the northeastern arm of Danu Montes, within Fig. 10. The mountains formed by crustal shortening along a series of thrust systems striking approximately parallel to the topographic trend. Numerous pits, graben, and collapsed troughs crosscut the thrusts and indicate both lateral extension generally perpendicular to the direction of thrusting and magmatism enabled by the crustal thickening and extension. The largest extensional feature in this region is a depression about 20 by 75 km in the center of the image; it is at an angle of about 30° to the topographic trend and occurs near the local topographic crest. The image is centered near 60°N, 337°E, and is 190 km wide.

the upper crust over a weak lower crust; for reasonable thermal gradients the slopes are sufficient for such sliding to be important (*33*). Extensional features oriented subparallel to the topographic trend and located near the crest of the mountain belt (such as that in Fig. 12) also have analogues in active terrestrial mountain belts (*34*) and could result from gravitational spreading or collapse of the mountain crest.

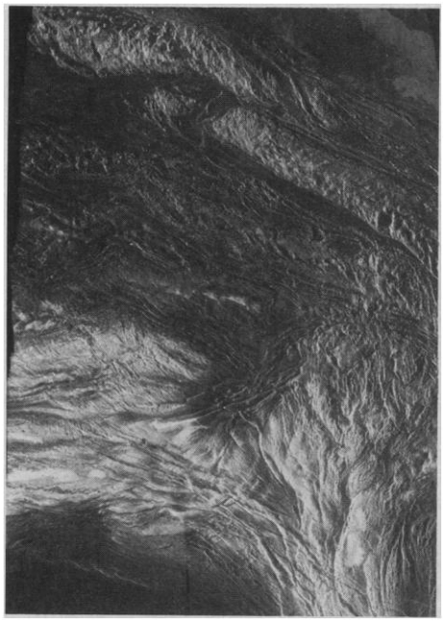

Fig. 13. Magellan radar image of central Freyja Montes. The image shows the radar-dark, somewhat deformed plains of northernmost Lakshmi Planum in the southwestern corner, the radar-bright high terrain of the mountain belt, the intensely deformed plateau of Itzpapalotl Tessera to the north of the high mountains, and the steep slope of Uorsar Rupes linking the plateau with the north polar plains visible in the NE corner of the image. The image is centered near 75°N, 336°E, and is 380 km wide at the base.

Magellan data for the central and eastern parts of Freyja Montes illustrate several important characteristics. In the central part of the belt (Fig. 13) the broad bright and dark bands observed in Arecibo and Venera images and trending parallel to the strike of the mountain belts (*5, 6*) are seen in detail in the Magellan images and are interpreted as broad ridges and troughs complexly deformed by a variety of structures. For example, a series of linear fracture-like discontinuities striking ENE disrupt the generally E-W–trending ridges and troughs, whereas parts of the E-W structures are cut by NW striking, closely spaced fractures and linear graben-like depressions up to several kilometers wide (Fig. 14A). Where relations between these two sets of features can be seen (Fig. 14A, point A), the NW-striking fractures curve toward the ENE striking fractures in S-like patterns, suggestive of shear along the latter structures. The most common sense of shear implied by this pattern is right-lateral. In several places within the mountain belt there are serrated patterns generally parallel to the topographic grain and consisting of rhomb-shaped radar-dark patches (Fig. 14A, point B, and Fig. 14B), which appear to be fault-bounded depressions. The rhombs have some similarities to pull-apart basins formed along some terrestrial strike-slip faults (*35*) and, if formed in an analogous manner, would imply right-lateral shear. Under this interpretation the most recent direction of crustal compression in central Freyja Montes has been oblique to the principal topographic trends of the mountain belt (most likely NNW-SSE to NW-SE), a phenomenon common in terrestrial mountain ranges (*36*). Alternatively, the rhombs could represent extension resulting from gravitational collapse of the high terrain of the mountain belt; the geometry may have been controlled by older ENE-trending fractures. The serrated pattern in Fig. 14B is on a steep south-facing slope, which would favor gravitational spreading.

South of the steep southern front of Freyja Montes are radar-dark plains of apparent volcanic origin sloping downward toward central Lakshmi Planum. Associated with these plains are a series of somewhat sinuous scarps parallel to the mountain front and first observed in Venera data (*13, 29*). Magellan data reveal that these features are characterized by en echelon patterns; the larger ones appear to be asymmetric, and their steep sides face toward Lakshmi Planum (Fig. 14A, point C, and Fig. 14B). These features are interpreted as the surface expressions of low-angle thrust faults. They most likely formed during the tilting of the volcanic plains and contemporaneously with the lithospheric shortening and crustal thickening accompanying formation of the mountain belt. Some of the thrust faults along the mountain flanks may also have formed or been reactivated during gravitational collapse of the mountain crest.

Evidence for volcanism within low flat valleys in the plateau of Itzpapalotl Tessera north of Freyja Montes includes long sinuous channels associated with volcanic plains; these plains are little deformed and clearly embay the complexly faulted mountains (Fig. 15). These relations suggest that some volcanism has postdated deformation in this region. The occurrence of relatively recent volcanism in Itzpapalotl Tessera, at an elevation comparable to Lakshmi Planum but

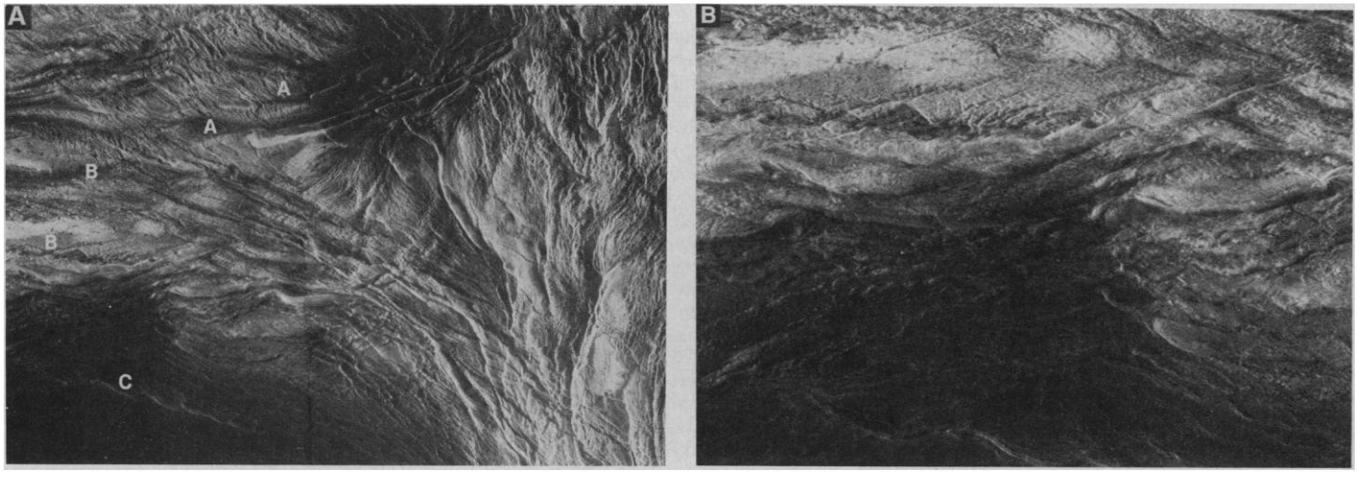

Fig. 14. Two expanded views of portions of Fig. 13. (**A**) The high-standing terrain of the central Freyja Montes belt. The image is centered near 74°, 336°E, and is about 330 km wide at the base. Lettered points are discussed in the text. (**B**) The transition from Freyja Montes southward to Lakshmi Planum is shown in this image, centered at73°N, 332°E, 140 km wide at the base, and within the area shown in (A). Both thrust faults and possible shear zones can be seen in the radar-bright upper portion of the image. Thrust faulting extends out onto the volcanic plain of Lakshmi Planum, which slopes to the south in this region. The range in elevation in this image is approximately 3 km.

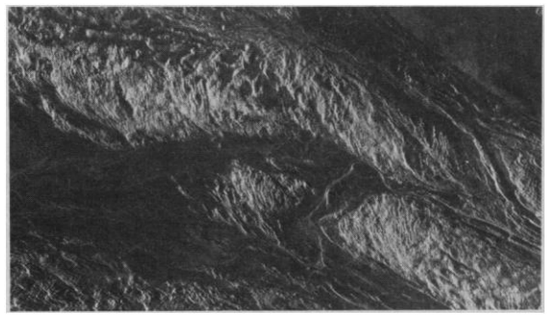

Fig. 15. This image, centered at 77°N, 337°E, and 260 km wide, shows part of the plateau north of Freyja Montes and, in the northeastern corner, the steep scarp of Uorsar Rupes that drops by about 3 km to the volcanic plains to the north. The plateau consists of elevated and highly faulted ridges and intervening smooth plains. A lava channel is evident running from east to west and indicates that the smooth plains are volcanic in origin. The plateau stands at about the same elevation as Lakshmi Planum to the south (Fig. 9B).

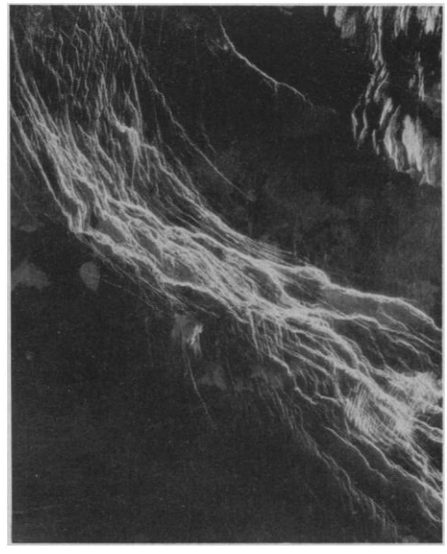

Fig. 18. An expanded view of the rift system extending southeastward from Gula Mons in western Eistla Regio. The steep-walled rift is 50 to 75 km wide, and the floor lies as much as 1 km below the rim. The image is centered at about 18°N, 1°E, and is about 410 km wide.

separated from it by the intervening mountain belt, is consistent with the hypothesis that at least some magmatism in Ishtar Terra is the result of remelting of thickened crust (*28, 29*) rather than pressure-release melting in a mantle plume beneath Lakshmi (*31*). In contrast to Danu Montes, no significant evidence for volcanic deposits or features (collapse pits, sinuous channels, ponded lava deposits) have been found in the imaged area of the higher parts of Freyja Montes.

Freyja Montes turn southward along the eastern edge of Lakshmi Planum, and the character of the mountain range changes (Fig. 16). The elevation decreases southward, and the rim and flanks of eastern Lakshmi Planum are characterized by abundant graben generally oriented parallel to the topography; patches of volcanic plains locally embay these graben at the base of the eastern Lakshmi margin. A large dome-like feature 100 by 150 km displays intersecting graben typically spaced 2 to 5 km apart. Flanking and surrounding this structure are ridges that appear to be thrust faults or folds. The dome-like feature may be previously high terrain that has gravitationally collapsed. The graben are disrupted where they intersect the ridges, suggesting that the ridges may be the result of thrusting at the periphery of the gravitationally collapsing high.

The generally N-S–trending eastern Freyja Montes appear to be dominated by extensional features with a variety of orientations; these structures suggest that this area is no longer undergoing active shortening but has more recently been subjected to significant gravitational collapse. The E-W–trending central Freyja Montes, in contrast, lack the abundant graben-like features typi-

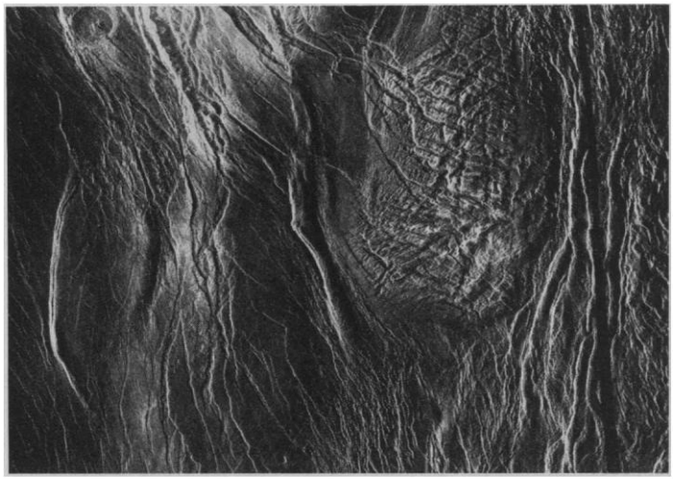

Fig. 16 (left). Magellan radar image of the southern portion of eastern Freyja Montes and of the eastern margin of Lakshmi Planum. The highest terrain is the radar-bright area in the upper left. Some of the N-S– trending compressive structures in the mountains and in the radar-dark plains of eastern Lakshmi Planum on the left probably date from the time of crustal shortening during mountain formation. The many extensional structures likely formed during a generally later period of gravitational collapse of high terrain. The image is centered at 71.5°N, 340°E, and is 250 km wide.

Fig. 17 (right). Magellan radar image of Gula Mons and associated tectonic features. The volcano summit is at the southwestern end of the 150-km-long, NE-trending, radar-bright zone in the center of the image. To the north of Gula is a corona-like feature about 200 km in diameter; several large lava flows appear to originate from within the feature. The image is centered at about 22°N, 359°E, and is about 750 km wide.

cal of eastern Freyja and show locally steep slopes and evidence of intense folding and shear. We suggest that crustal shortening and thickening across central Freyja Montes has continued until geologically recent time.

Volcanic rises. Broad topographic rises dominate the equatorial regions of Venus. Collectively referred to as the equatorial highlands (*37*), they include Aphrodite Terra and Asteria, Beta, Eistla, and Phoebe Regiones. These rises tend to occur in linear to arcuate belts but individually are circular to quasi-circular in planform. Associated with the rises are rift zones 100 to 300 km wide and up to thousands of kilometers in length as well as large volcanic constructs and their attendant lava flow fields (*3, 7, 8, 38*); hence, we refer to them here as "volcanic rises." The apparent depths of isostatic compensation for volcanic rises are typically between about 100 and 200 km (*39*); such depths imply that at a regional scale the topography is at least partly supported by mantle dynamic processes (*37, 40*).

Some workers have proposed that volcanic rises are made up of one or more hot spots, that is, they are the surface expressions of large areas of mantle upwelling (*40*). Others have suggested that the rises of the Aphrodite Terra region are also centers of significant crustal spreading (*41*). In the hot-spot model the broadly elevated topography of a volcanic rise is the result of uplift asociated with buoyancy forces from both the underlying mantle upwelling and the thermally thinned lithosphere (shorter wavelength topography may be associated with magmatic processes). Magellan imaging data offer the opportunity to test the hypothesis of dynamic uplift by searching for the attendant tectonic signatures. The task will be difficult because there ought to be several stages of deformation associated with even the early evolution of a hot spot, and volcanism is likely to obscure much of the tectonic evidence of prior episodes of activity.

Only one volcanic rise lies even partly within the area covered by the first month of mapping: western Eistla Regio, an elongated (2000 by 3000 km), NW-trending topographic high. Western Eistla Regio stands about 1 km above a 6052-km datum and is capped by two volcanic constructs, Sif Mons and Gula Mons, which rise about 2 and 4 km above this reference level, respectively. A significant long-wavelength positive gravity anomaly characterizes this region, and the apparent depth of compensation is 100 to 200 km (*39, 42*). In the vicinity of Sif Mons at least four distinct volcanic units can be mapped, and the major tectonic features seen there apparently postdate the two oldest units (*12*).

The dominant tectonic style observed in western Eistla Regio is extensional (Fig. 17). The most prominent tectonic features consist of two parallel en echelon sets of NW-trending normal faults and graben, one set intersecting Gula Mons and another to the west of the first intersecting Sif Mons. The eastern fault system is best developed along the summit trough of a broad linear rise extending southeast of Gula Mons for more than 1000 km toward Sappho Patera (Fig. 18). The rise is 700 km or more in width and stands 500 m or more above the surrounding terrain; the summit trough is 50 to 75 km wide and up to 1 km or more in relief (*12*). The faults and graben, spaced a few to a few tens of kilometers apart, are concentrated along the floor and inner walls of the trough. We interpret the trough as a rift resulting from significant stretching and thinning of the lithosphere. The rift has dimensions, relief, and fault characteristics similar to rift systems in other equatorial highland regions (*3, 7*).

A number of additional faults and lineations are associated with the two major volcanoes. Radial fractures and normal faults are observed to extend outward from Gula Mons 400 km or more; several normal faults and graben run NE along the radar-bright summit (Fig. 17). To the NW of Gula Mons, the NW-striking fractures merge into a set of faults concentric to a corona-like feature (see below) about 200 km in diameter; the interior of this feature is elevated at least 500 m, and several prominent lava flows appear to flow northward from topographic embayments within the main structure. Some of the faults concentric to the corona-like feature cut, and are therefore younger than, the fractures radial to Gula Mons. An additional set of lineations extends outward from the summit of Gula Mons and bends southward. These lineations, which on the basis of their narrow widths and geometry may be the surface expressions of dike systems, are best developed to the west, NW, and SE of the volcano; elsewhere they appear to be buried by younger lava flows. Several normal faults and graben of the southeastern rift system appear to terminate or step across one or more of the curved lineations; these relations indicate that some extension across the rift postdated formation of the curved lineations.

At Sif Mons, the most prominent faults are those to the NW and SE and constitute a fracture pattern paralleling the dominant fabric observed at Gula Mons [figure 4C in (*12*)]. Some radial faults partly buried by volcanic flows may also be seen to the west, southwest, east, and north. The fault systems around Sif Mons extend for at least 500 km and possibly 1000 km to the NW and almost 400 km to the SE, where they disappear just short of the radial system striking southwestward from Gula Mons.

The geometry of rifting and volcanism suggest that the least compressive horizontal stress has most recently been oriented approximately NE-SW. The smaller scale tectonic features in the Sif and Gula Mons regions may reflect older stress systems, possibly related to the formation of the large volcanic shields. Some of these local faults may have been reactivated by the NE-SW–oriented extensional stress field and in turn may have served to focus the intensity of the

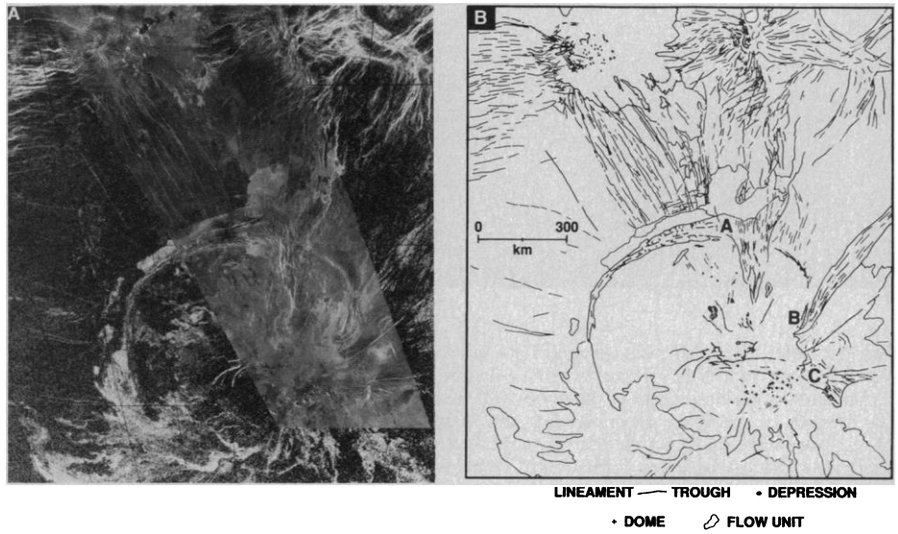

Fig. 19. (**A**) Arecibo radar image (*9*) of the corona Quetzalpetlatl (*45*) and its surroundings with an inset of the higher resolution Magellan image coverage mainly over the eastern half of the corona. Quetzalpetlatl is about 800 km in diameter and centered near 68°S, 355°E. A smaller 160-km-diameter corona-like feature can be seen in the upper left corner. (**B**) Geologic sketch map of the image in (A). Points A, B, and C indicate features discussed in the text. Map prepared by E. R. Stofan.

regional scale deformation in the vicinity of the volcanoes. Whether the volcanism at Sif Mons and at Gula Mons is at least partly a passive response to lithospheric stretching or, alternatively, the extension is secondary to hot-spot volcanism and regional uplift, remains to be determined. If the apparent depth of compensation of topography is in the upper part of the range of current estimates (*39, 42*), however, then active mantle upwelling must be involved. Because the extension is approximately orthogonal to the regional topography, simple spreading of western Eistla Regio in response to crustal stresses associated with both elevation variations and lithospheric lateral density gradients must also be considered. There is no tectonic signature that can be unambiguously assigned to the formative stage of western Eistla Regio as a whole and therefore no clear test of the hypothesis of large-scale dynamic uplift. Probably the tectonic manifestation of the earliest history of western Eistla Regio has long since been destroyed by volcanic resurfacing.

Coronae. Coronae are circular to elliptical structures surrounded by an annulus of concentric ridges (*4, 5*). Found only on Venus, they are characterized by relatively elevated topography, interior and exterior volcanism, interior extensional and compressional tectonic features, and a peripheral trough (*4, 5, 43, 44*). Particular coronae may lack or display only partially one or more of these characteristics. Coronae have been interpreted to be products of plume-like upwelling of the Venus mantle (*5, 43, 44*), presumably on a scale more localized than the postulated upwelling beneath the comparatively broader volcanic rises.

Magellan has obtained high-resolution images and topography of a part of one of the largest coronae on Venus, Quetzalpetlatl (*45*), an asymmetric corona about 800 km in diameter centered at about 68°S, 355°E, in northern Lada Terra. On the basis of Arecibo data, it was concluded that along its northwestern edge this corona has a partial annulus of ridged terrain and an outer moat partially infilled with lava, and that offset to the southeast from the center of the corona is a large radar-dark interior region of extensive lava flow units, perhaps a complex caldera; narrow, radar-bright lineations hundreds of kilometers long and oriented approximately radially to the corona were identified as possible scarps and faults (*9*). The high-resolution Magellan images and topographic data show that the annulus of ridged terrain (Figs. 19 and 20) actually consists of several circumferential ridges separated by lower lying, volcanically flooded areas.

The structure and width of the annulus are highly variable. In the north-northwestern sector of the corona the width of the annulus is about 50 to 75 km. The peripheral trough along the corona margin in this sector is comparable in width to the annulus of ridges and appears to be no more than a few hundred meters deeper than the plains to the northwest (Fig. 21). The trough is flooded with lavas whose sources may be adjacent to the annulus and, in particular, associated with fractures along the northern margin of the corona. The major topographic expression of the corona along the northwestern margin is its abrupt rise by more than 500 m over a horizontal distance of about 75 km; the position of the rise is approximately coincident with the annulus of ridges (Fig. 21).

The lava-filled trough on the northwestern margin of Quetzalpetlatl is superposed on the fractures extending northwestward from the corona (Figs. 19 and 20). These fractures are graben that in many places consist of short segments with en echelon offsets (Fig. 20). The radial fractures cut a series of circumferential graben exterior to the trough on the northwestern boundary of the corona (Fig. 20). In a few instances the fractures can be discerned through the lava flows infilling the peripheral trough. The extensive volcanic deposits in the corona interior also largely cover the NW-striking radial fractures there, although a few can be seen.

The eastern and southern margins of Quetzalpetlatl differ significantly from the northwestern margin. To the NNE (point A, Fig. 19B), circumferentially oriented features are fractures rather than ridges, and the fractures both cut and are cut by a set of NNE-striking radial fractures. These fractures are distinct from those striking NW exterior to the corona. Spacings between these fractures are no more than the widths of individual features, approximately 2 to 5 km, in contrast to the NW-striking fractures on the northwestern margin, which are narrower (about 1 km wide) and spaced approximately 35 to 55 km apart. The NNE-striking fractures are part of a regional set of linear features that cut the corona and postdate the volcanism in the corona interior

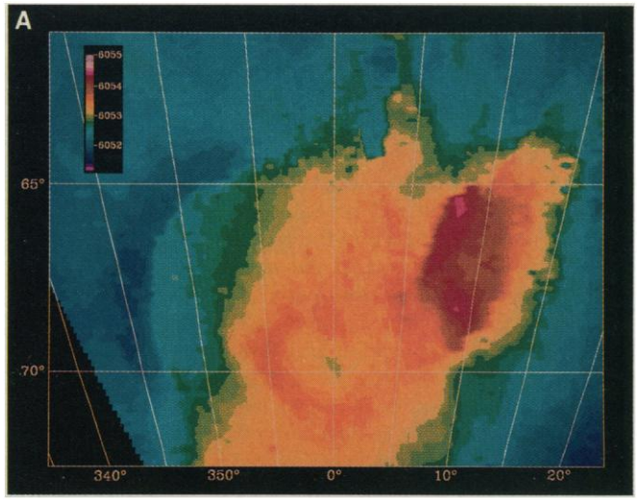

Fig. 21. Color-contoured Magellan altimetry of Quetzalpetlatl corona and surrounding regions; contours are planetary radius in kilometers.

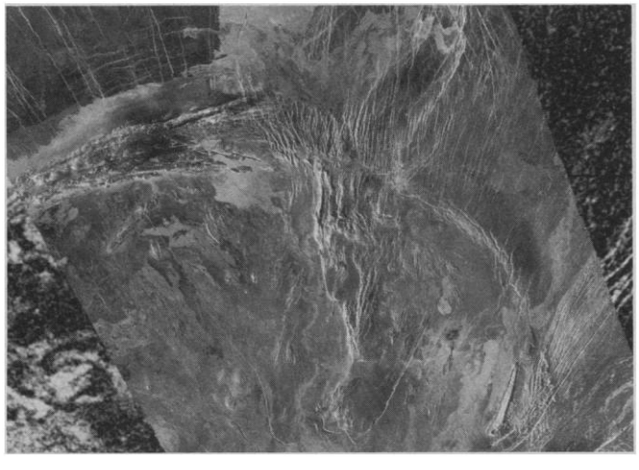

Fig. 20. An expanded view of Fig. 19A in the vicinity of the northern rim of Quetzalpetlatl corona. The image is centered at about 66°S, 0°E, and is about 700 km wide.

(Fig. 19). They extend into the corona in contrast to the NW-striking fractures, which are covered by volcanic deposits. The northeastern margin of Quetzalpetlatl consists dominantly of a single broad, concentric ridge, in places cut by concentric and obliquely striking fractures. The broad ridge or swell is approximately 25 km across. Belts of parallel troughs cut parts of the ridge but are overlain by lava flows in the interior (Figs. 19 and 20 and at points B and C, Fig. 19B). The belts of troughs are interpreted to be extensional in origin and to have formed contemporaneously with the corona. To the south, only flow deposits of apparent volcanic origin can be seen in Arecibo or Magellan images, with no evidence for a ridge or annulus.

The overall topography of the corona is approximately that of a dome; the interior of the corona rises more than 1 km above the surrounding plains (Fig. 21). The northwestern quadrant of the corona, however, is more plateau-like. The eastern margin lies along the edge of a steep topographic rise, approximately 1 km high, associated with a regionally extensive zone of NE-striking fractures, graben, and pit chains. Southeast of the center of the corona is an elliptical low, about 200 km across and up to 500 m deep. This low approximately corresponds to the volcanic source region identified in Arecibo images of the corona (*9*). Concentrated in and around this low region are numerous bright and dark flows and small (0.5 to 20 km) volcanic domes [Fig. 19; see also figure 19 in (*12*)]. A zone of arcuate fractures parallels topographic contours in this region, approximately defining the edge of the topographic low. We interpret these fractures to be caused by flexure or downdropping of the surface of the corona as a result of magma withdrawal, similar to the fracturing associated with Sacajawea Patera (*12*).

Except for the annular ridges and some tectonic ridges and patches of high-standing fractured terrain in the interior, the corona is everywhere covered by radar-bright and -dark lobate plains units interpreted to be lava flows from widely distributed sources (Fig. 19). Volcanic deposits are widespread and varied in style (*12*); extensive flow units (up to 500 km long), possible collapsed lava tubes, calderas, small volcanic domes, and diffuse dark deposits are all visible within the interior.

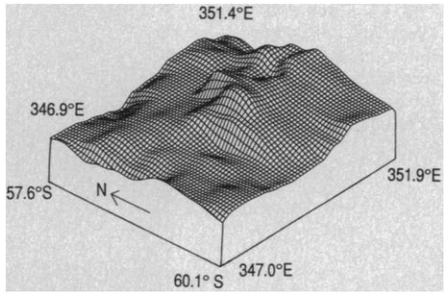

Fig. 23. Three-dimensional representation of the topography of the corona-like feature of Fig. 22.

The tectonic features and relations discussed above suggest the following stages in the development of this corona: uplift and radial fracturing (including the NW-striking fractures), formation of the exterior trough and the annular ridges (visible only on the northwestern margin) or ridge (along the eastern margin), widespread volcanism, and further regional deformation and volcanism. There may also have been volcanic activity contemporaneous with the earliest deformation, but any such flows must be buried beneath the later volcanic deposits that embay the radial fractures interior to the corona and both embay and cover the annular ridges. Formation of the annulus of ridges must have postdated the radial fracturing associated with the initial uplift because the NW-striking radial fractures are overprinted by the annulus. In general, the volcanic and tectonic history outlined above is similar to those suggested for the coronae visible in Arecibo and Venera 15–16 data and is consistent with corona formation above a hot plume of localized mantle upwelling impinging on the base of the lithosphere (*19, 43, 44*).

About 1100 km to the northwest of the center of Quetzalpetlatl is a smaller corona-like feature centered at 59°S, 350°E, on the southern margin of Lavinia Planitia (Fig. 19). This quasi-circular feature is a structure of complex faulting, volcanic flows, mounds, and pit craters about 160 km in diameter (Fig. 22). Radial and concentric faults are prominent only in the western and southwestern parts, which also are characterized by radially oriented lava flows. The eastern part of the feature is dominated by volcanic plains contiguous with the plains exterior to the structure. Both the interior and exterior plains contain lava channels and numerous small domical mounds topped with central pits (*12*). The feature lies at the intersection of two broad regional fracture trends, one extending south-southeast towards Quetzalpetlatl and another extending to the east and west (Fig. 19).

Altimetry data show that the feature (Fig. 23) coincides with a broad, gentle topographic dome. The summit lies near the center of the feature and more than 500 m above the plains to the north and west but only about 100 m above a broad plateau to the east and southeast. There is no indication in the altimetry of a central depression or of a bounding annular ridge or moat.

The concentric lineations that partially define the structure consist in some areas of graben that vary in width from the limit of resolution to as much as 2 km across. Concentric graben are best developed in the southwestern part of the structure. In the northwestern part, some of the concentric lineations are radar-bright features interpreted to be step faults downdropped to the WNW, whereas others are clearly graben.

Radial lineations are particularly well developed in the northwestern and southwestern sectors. The northernmost ones, trending WNW, appear to be shallow, broad (approximately 2.5 km wide) graben that are cross-cut and truncated at their proximal (southeastern) ends by younger concentric structures. At the distal ends of these radial

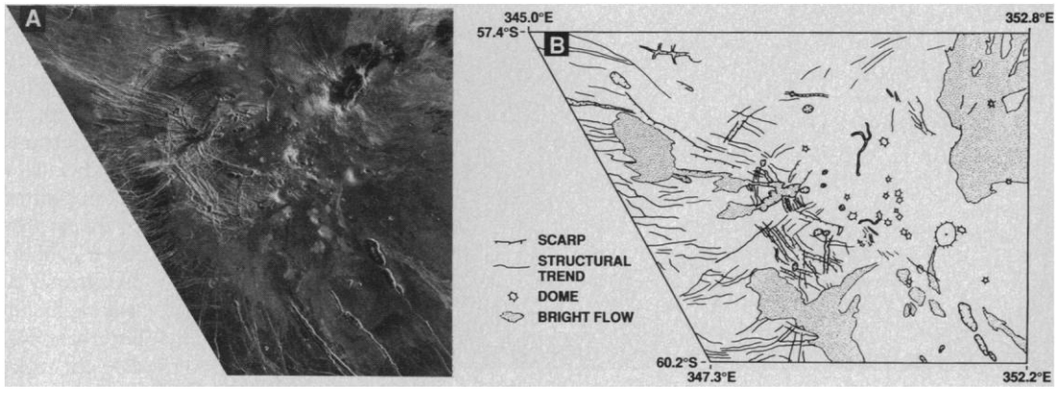

Fig. 22. (**A**) Magellan radar image of a corona-like feature located about 1100 km north of Quetzalpetlatl corona. The feature is centered at about 59°S, 350°E. The top of the image is 390 km wide. The irregularly shaped radar-dark region in the upper right of the image and the three elongate depressions in the lower right are volcanic features (*12*). (**B**) Geologic sketch map of the corona-like feature in (A). Map prepared by S. W. Squyres.

fractures, the concentric fractures appear older.

The history of this feature appears to have been one of uplift, radial and concentric fracturing of the surface, and volcanism. The oldest fractures, as deduced from crosscutting relationships, appear to be radial and are cut or terminated by concentric features. Some of the youngest fractures, however, also have radial orientations and cut through the western part of the structure. Some of the younger radial fractures are aligned with lines of pit craters and volcanic flow sources. Volcanism apparently occurred throughout much of the history. The earliest visible volcanic units flooded the interior, as well as the plains to the east, west, and south. Later, after the formation of the concentric faults, additional lavas erupted to form the channeled flows that cross the structure to the west. The final episode of volcanism appears to have been the development of the numerous small volcanic mounds in the center and to the east of the structure.

What is the relation of this feature to coronae? It is circular and clearly not of impact origin, but unlike many coronae, it lacks an outer annulus of ridges. Although volcanic forms are abundant the exposed interior radial and concentric fracturing is more evident than in most coronae observed to date. A possible interpretation is that this feature is either an incipient or failed corona. In the early stages of corona formation, according to the mantle plume scenario, both fracturing and volcanism would be expected; later stages could include extensive flooding and gravitational relaxation (*43, 44*). For this feature, however, development may have progressed only to the point of uplift and somewhat limited volcanism.

Tessera. Tessera terrains are broad regions characterized by two or more sets of intersecting linear features (*5, 19*). These linear features generally appear to be the manifestations of ridges, troughs, and scarps formed as a result of tectonic deformation. Tesserae cover approximately 15% (*46, 47*) of the northern high latitudes (north of 30°N) imaged by the Venera 15–16 orbiters at 1 to 3 km resolution and have also been observed at lower northern and at southern latitudes in radar images at 1-km resolution obtained at the Arecibo Observatory (*9*). Tessera terrain generally stands 1 to 2 km higher than surrounding plains and is characterized by high surface roughness at meter and submeter scales (*48*). On the basis of these characteristics, Pioneer Venus data on surface roughness and reflectivity suggest that tessera are widespread throughout parts of Venus not yet observed at high (1 km or better) resolution (*49*). Known large areas (1000 km or greater in width) of tessera display a relatively shallow (<100 km) apparent depth of compensation (*39, 50*). This characteristic contrasts with the large apparent depths of compensation indicated for most large-scale topographic features on Venus and suggests that most tesserae are compensated primarily by enhanced crustal thickness rather than mantle dynamic processes. Hypotheses for the formation of tessera terrain include gravity sliding (*46, 51*), interaction between mantle plumes and crustal spreading centers (*52*), late-stage deformation of elevated regions of thick crust (*53*), and a combination of crustal compression and subsequent gravitational relaxation (*54, 55*).

Within the area mapped during the first month of the Magellan mission, the largest expanse of tessera terrain is Alpha Regio, an upland area polygonal in outline, approximately 1300 km across, and centered at about 24°S, 4°E. In general Alpha Regio stands 1 to 2 km above the surrounding plains, but the topographic relief ranges locally up to 5 km (Fig. 24A). In Arecibo images at 1-km resolution the region is characterized by radar-bright and dark lines forming complex arcuate and linear patterns and interpreted to represent structural ridges and troughs, and numerous dark regions 20 to 100 km across that are interpreted as smooth plains of volcanic origin. Magellan images of western and central Alpha Regio resolve these features and permit the identification of sequences of tectonic and volcanic events, styles of deformation, and structural and morphologic units.

Along the margin of Alpha Regio with the extensive plains to the west (Fig. 24) are a set of broad, N-S–trending ridges and scarps striking generally parallel to topographic contours. These broad ridges and scarps are spaced about 10 to 20 km apart and are laced by closely spaced parallel grooves and ridges about 200 to 800 m apart. Plains of apparently volcanic origin embay these features at the western edge of Alpha, and patches of plains occur at various elevation levels to the east. Thus, volcanism has postdated the latest structural deformation in this part of the tessera.

Tectonic patterns within the tessera are complex. A generally orthogonal pattern of structures occurs as part of a broad NW-trending zone (Fig. 24C). This terrain is characterized by a pattern of relatively long (typically >50 km) zones of disruption that commonly appear to crosscut shorter (<25 km) scarps, grooves, and graben at angles near 90°. Disruption zones trend approximately WNW, whereas the shorter features trend NNE. Some disruption zones appear to be troughs approximately 20 to 50 km wide. In some areas the individual shorter features are observed to cut through the disruption zones. This orthogonal terrain is similar to trough-and-ridge terrain identified in tessera units from Venera data (*54*) in terms of orientations, spatial scales, and morphology of structures.

Other parts of Alpha are dominated by curvilinear patterns (Fig. 24D), characterized by multiple linear and curvilinear structures at scales ranging from about 20 km down to the limit of resolution. The largest structures are arcuate ridges and troughs about 10 km wide and no more than 70 km long. Some of these structures are nearly linear whereas others are sharply curved, with radii of curvature of less than 50 km. Smaller structures include ridges, troughs, and scarps spaced 400 to 800 m apart, and somewhat larger graben, approximately 5 km wide and up to several tens of kilometers in length. The smaller structures most commonly intersect the broader ridges and troughs at a variety of angles and in fewer cases are aligned with the broader features. Graben trending NW and N-S crosscut most other structures and thus appear to represent the latest phase of deformation in the area. The NW-trending graben are found throughout most of west-central Alpha, with the exception of the belt of orthogonal terrain. Broad ridges and troughs in this somewhat chaotic terrain are similar in size and relative orientations to structures that define disrupted terrain observed in Venera images of tessera (*54*).

Magellan images of Alpha Regio reveal details of structure and fine-scale deformation not apparent in earlier lower resolution data. Embayment of ridged and disrupted ridged terrain by volcanic plains and subsequent deformation of some of these plains in central Alpha indicate that volcanism and tectonism were temporally interleaved and that some volcanism locally postdates deformation. Similarly, structures within Alpha (Fig. 24, B to D) exhibit crosscutting relations that define a complex series of tectonic events; the style of deformation probably varied with both location and time. More regional coverage and detailed analysis will help to decipher this sequence. NW-trending graben crosscut almost all units in central Alpha; comparatively recent extension may have been responsible for their formation.

In general, tessera terrain appears to record intense and broadly distributed deformation at a range of spatial scales. We interpret this pervasive deformation as evidence for significant horizontal and perhaps vertical strain, probably involving primarily ductile deformation of much of the crust and brittle deformation at least at times of only a thin surficial layer. The complexity of

superposed tectonic patterns in most tessera regions imaged by Magellan to date suggests that such areas have experienced multiple episodes of deformation. There likely are a variety of evolutionary paths by which regions of elevated topography and thickened crust can sustain the intense deformation now manifested in the different forms of tessera terrain.

Generalizations. Magellan images and altimetry show that both horizontal shortening and horizontal extension have occurred widely on the Venus surface at a variety of scales, ranging from the 1-km scale that characterizes the spacing between tectonic features in a number of regions to the 1000-km scale that governs the large-scale physiography of major structures and the spatial coherence of many smaller scale patterns of strain. Evidence for shear is present in the ridge and groove belts and in the mountain belts, but the shearing tends to be broadly distributed and to accompany horizontal stretching or shortening. No clear examples have yet been documented of long, large-offset strike-slip faults such as those typical of oceanic and many continental areas on Earth.

The various scales of deformation arise from the complicated mechanical and dynamical structure of the Venus interior. The 10- to 30-km scale is plausibly attributed to the response of a strong upper crustal layer, whereas the deformation of a strong upper mantle layer can account for tectonic features with characteristic scales of a few hundred kilometers (*16*). The scale of a few hundred to a few thousand kilometers, particularly if evident in the long-wavelength gravity as well as the topography, is likely dominated by mantle convection and its associated dynamic stresses and heat transport. The scale of a few kilometers and less involves either internal deformation of the upper crust or tectonic disruption of a thin surficial layer decoupled thermally or mechanically from the remainder of the otherwise strong upper crust.

Venus displays several geometrical variations on lithospheric extension and associated volcanism. The coronae, quasi-circular in planform, involve modest increases in sur-

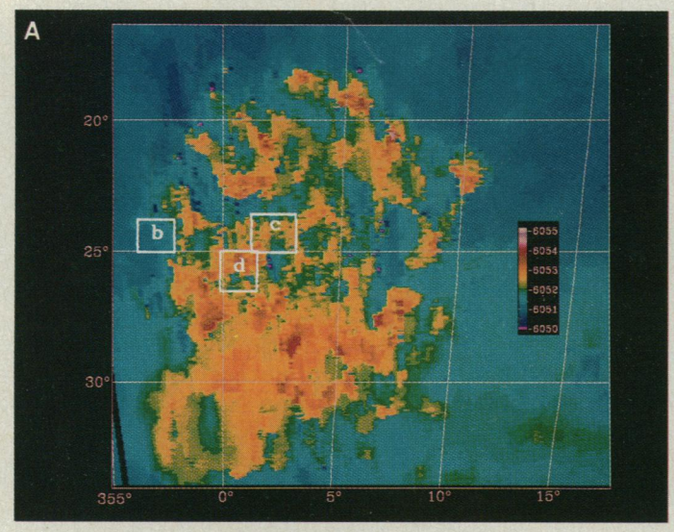

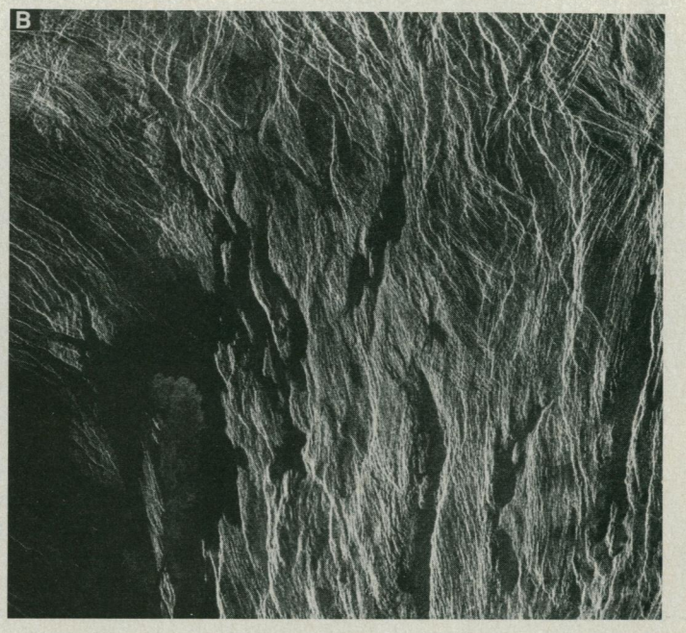

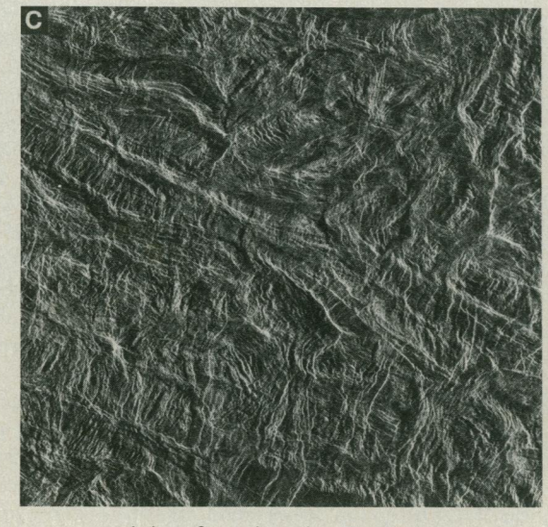

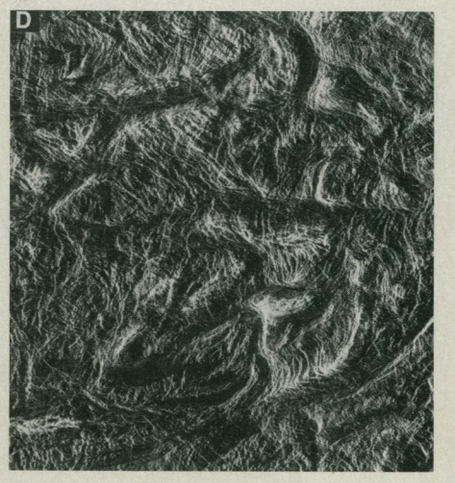

Fig. 24. (**A**) Color-contoured Magellan altimetry of Alpha Regio and surrounding plains; the locations of the images shown in (B to D) are shown by boxes. (**B**) Magellan radar image of a portion of the western edge of the tessera of Alpha Regio and of its boundary with the surrounding lowland plains. The image is about 100 km wide and is centered at 24.5°S, 357°E. Elevation increases by approximately 1 km from the dark smooth plains in the lower left to the eastern edge of the frame. Toward the north, N-S–trending ridges and scarps are commonly crosscut by NW-trending graben. (**C**) Magellan radar image of orthogonally patterned terrain in Alpha Regio. The image is about 150 km wide and is centered at 24.5°S, 2°E. NNE-trending structures, consisting primarily of graben, are spaced about 1 km apart and are less than 25 km long. Longer (>50 km), more widely spaced (20 to 50 km) structures consisting of troughs and ridges trend WNW and commonly crosscut smaller NNE-trending structures. (**D**) Magellan radar image of complex tessera terrain within Alpha Regio. The image is about 150 km wide and is centered at 25.5°N, 1°E. As in the orthogonally patterned region (C), two scales of structures are evident. The first, at a spacing of 10 to 20 km, consists of ridges and troughs arranged in arcuate, loop-like patterns. The second, at a spacing of 1 km or less, consists of graben, fractures, and scarps displaying both regional trends (such as the NW-trending graben) and local trends related to the broader ridges and troughs.

face area and large volumes of volcanic deposits. Such features are thought to be the products of transient plumes of upwelling mantle material. Broad rises with linear rift zones are permissive of greater degrees of lithospheric extension and thus greater rates of magma generation (*56*). Such rises are also thought to be sites of mantle upwelling, on the basis of the large apparent depths of compensation of long-wavelength topography, but the relative lifetimes and buoyancy fluxes of postulated upward flows beneath broad rises and coronae has not been closely examined. Extensional fault systems, and large rift systems in particular, may show a tendency for self-erasure, in that significant lithospheric stretching should lead to pressure release melting in the mantle and volcanism that will act to bury the tectonic evidence for extension. In western Eistla Regio, for instance, the rift system to the southeast of Gula Mons may have once continued for several hundred kilometers to the northwest; if so it is now buried by the volcano and its associated flows.

Horizontal compression on Venus is manifested in features ranging from wrinkle ridges, to elevated deformation belts, to the great linear mountain belts. In general compressive features are more evident than extensional features in the areas viewed to date by Magellan. To some extent this is coincidental, in that there are many large highland regions thought to be sites of lithospheric extension that have yet to be imaged. The prevalence of compressive structures, however, may be in part because compression is accompanied by crustal thickening and uplift, and the elevated terrain is less susceptible to resurfacing by volcanic burial. In the absence of significant weathering and erosion, the lifetime of high topography is limited by ductile flow in the thickened lower crust that must at least partly support the topographic relief once active compression ceases. Numerical models suggest that mountain belts on Venus, in the absence of ongoing dynamic support, may have lifetimes of 100 million years or less (*57*), and the widespread evidence for lateral extension in the mountains of Ishtar Terra documents the tendency for such ductile flow to occur. Ishtar Terra, of course, is not typical terrain, in that mountain belts have not been observed elsewhere on Venus, and the steep slopes marking some of the edges of Lakshmi Planum and the front ranges of the mountain belts provide evidence that dynamical processes have been recently operative.

We have seen no evidence to date for tectonic behavior similar to Earth's oceanic regions, which are characterized by nearly rigid lithospheric plates with horizontal dimensions of 10^3 to 10^4 km and active deformation confined to narrow plate boundary zones a few kilometers to tens of kilometers across. Nor have we seen analogues to oceanic fracture zones or to deep sea trenches. Rather much of the tectonic behavior on Venus appears to be more reminiscent of actively deforming continental regions on Earth: deformation is distributed across broad zones one to a few hundred kilometers wide separated by comparatively stronger and less deformed blocks having dimensions of hundreds of kilometers. On Earth, the continental lithosphere in tectonically active areas is weaker than typical oceanic lithosphere because of the greater thickness of more easily deformable crust. Because of the higher surface temperature on Venus (740 K), the likely comparable lithospheric thermal gradients on Venus and Earth (*58*), and the strong temperature dependence of ductile behavior, the lithosphere on Venus should behave in a weak manner for crustal thicknesses less than are typical of continental regions on Earth (*33*).

In general, the intensity of deformation and state of preservation of tectonic features on Venus are strong functions of local topographic relief. Many elevated regions are areas of thicker crust and therefore a thicker layer of weak lower crustal material susceptible to ductile flow. Such regions thereby serve as concentrators of regional lithospheric strain, such as the ridge and groove belts in the lowlands and the mountain belts at the margins of Lakshmi Planum. Elevated regions, particularly areas elevated by compression and crustal shortening, are also less susceptible to volcanic resurfacing and thus are more likely to preserve records of deformation spanning one or more episodes of significant strain. Much of the surface of Venus may have only two possible fates: volcanic burial and comparatively long-term preservation as relatively elevated and repeatedly deformed terrain. The first fate is represented by the abundant volcanic plains; the second may be primarily represented by tessera terrain.

Despite the detailed view of the tectonic features of Venus that Magellan is providing, this view is yet of only a modest fraction of the planet's surface. Most of the broad questions to be answered about the tectonic history of Venus—the modes and rates of crustal formation, the global heat flux and its regional variations, the relative importance of localized hot spots and linear centers of crustal spreading to magmatism and tectonics, and the nature of mantle convection and its relation to lithospheric deformation and to magmatism (*58*)—must await global coverage of radar images, altimetry, and gravity by Magellan. Also required will be a new generation of quantitative models of interior processes capable of predicting characteristics with an information content comparable to that which Magellan is now providing.

REFERENCES AND NOTES

1. G. H. Pettengill *et al.*, *J. Geophys. Res.* **85**, 8261 (1980).
2. H. Masursky *et al.*, *ibid.*, p. 8232.
3. G. E. McGill, S. J. Steenstrup, C. Barton, P. G. Ford, *Geophys. Res. Lett.* **8**, 737 (1981); G. G. Schaber, *ibid.* **9**, 499 (1982).
4. V. L. Barsukov *et al.*, *Geokhimiya*, no. 12, 1811 (1984).
5. V. L. Barsukov *et al.*, *Proc. 16th Lunar Planet. Sci. Conf.*, *J. Geophys. Res.* **91**, D378 (1986).
6. D. B. Campbell, J. W. Head, J. K. Harmon, A. A. Hine, *Science* **221**, 644 (1983).
7. ———, *ibid.* **226**, 167 (1984).
8. D. B. Campbell *et al.*, *ibid.* **246**, 373 (1989).
9. D. B. Campbell, D. A. Senske, J. W. Head, A. A. Hine, P. C. Fisher, *ibid.* **251**, 180 (1991).
10. R. E. Arvidson, J. J. Plaut, R. F. Jurgens, R. S. Saunders, M. A. Slade, *Proc. 20th Lunar Planet. Sci. Conf.* **20**, 557 (1990).
11. R. S. Saunders *et al.*, *Science* **252**, 249 (1991).
12. J. W. Head *et al.*, *ibid.*, p. 276.
13. A. L. Sukhanov *et al.*, *U.S. Geol. Surv. Misc. Invest. Ser. Map I-2059* (1989); G. G. Schaber and R. C. Kozak, *U.S. Geol. Surv. Open-File Rep. 90-24* (1990).
14. E. R. Stofan, J. W. Head, D. B. Campbell, *Lunar Planet. Sci.* **21**, 1208 (1990).
15. D. L. Turcotte and G. Schubert, *Geodynamics* (Wiley, New York, 1982).
16. M. T. Zuber, *Proc. 17th Lunar Planet. Sci. Conf.*, *J. Geophys. Res.* **92**, E541 (1987); M. T. Zuber and E. M. Parmentier, *Icarus* **85**, 290 (1990).
17. H. S. Carslaw and J. C. Jaeger, *Conduction of Heat in Solids* (Oxford Univ. Press, Oxford, ed. 2, 1959).
18. J. B. Plescia and M. P. Golombek, *Geol. Soc. Am. Bull.* **97**, 1289 (1986); T. R. Watters, *J. Geophys. Res.* **93**, 10,236 (1988).
19. A. T. Basilevsky *et al.*, *Proc. 16th Lunar Planet. Sci. Conf.*, *J. Geophys. Res.* **91**, D399 (1986).
20. S. L. Frank and J. W. Head, *Earth Moon Planets* **50/51**, 421 (1990).
21. A. L. Sukhanov and A. A. Pronin, *Proc. 19th Lunar Planet. Sci. Conf.* **19**, 335 (1989).
22. J. Suppe, *Principles of Structural Geology* (Prentice-Hall, Englewood Cliffs, NJ, 1985), p. 275.
23. J. Jackson and D. McKenzie, *Geophys. J. R. Astron. Soc.* **77**, 185 (1984).
24. L. S. Crumpler, J. W. Head, D. B. Campbell, *Geology* **14**, 1031 (1986).
25. J. W. Head, *ibid.* **18**, 99 (1990).
26. ———, R. W. Vorder Bruegge, L. S. Crumpler, *Geophys. Res. Lett.* **17**, 1337 (1990); S. C. Solomon and J. W. Head, *ibid.*, p. 1393.
27. W. S. Kiefer and B. H. Hager, *Lunar Planet. Sci.* **20**, 520 (1989).
28. D. L. Bindschadler, G. Schubert, W. M. Kaula, *Geophys. Res. Lett.* **17**, 1345 (1990).
29. K. M. Roberts and J. W. Head, *Earth Moon Planets* **50/51**, 193 (1990).
30. R. E. Grimm and R. J. Phillips, *Geophys. Res. Lett.* **17**, 1349 (1990).
31. A. A. Pronin, *Geotectonics* **20**, 271 (1986); A. T. Basilevsky, *ibid.*, p. 282.
32. R. Armijo, P. Tapponnier, J. L. Mercier, T. L. Han, *J. Geophys. Res.* **91**, 13,803 (1986).
33. S. E. Smrekar and R. J. Phillips, *Geophys. Res. Lett.* **15**, 693 (1988).
34. B. C. Burchfiel and L. H. Royden, *Geology* **13**, 679 (1985).
35. A. G. Sylvester, *Geol. Soc. Am. Bull.* **100**, 1666 (1988).
36. A. Y. LeDain, P. Tapponnier, P. Molnar, *J. Geophys. Res.* **89**, 453 (1984); J. S. Oldow, A. W. Bally, H. G. Avé Lallement, *Geology* **18**, 911 (1990).
37. R. J. Phillips, W. M. Kaula, G. E. McGill, M. C. Malin, *Science* **212**, 879 (1981).
38. B. A. Campbell and D. B. Campbell, *Geophys. Res.*

Lett. **17**, 1353 (1990); D. A. Senske, *Earth Moon Planets* **50/51**, 305 (1990).
39. S. E. Smrekar and R. J. Phillips, *Earth Planet. Sci. Lett.*, in press.
40. R. J. Phillips and M. C. Malin, in *Venus*, D. M. Hunten, L. Colin, T. M. Donahue, V. I. Moroz, Eds. (Univ. of Arizona Press, Tucson, 1983), pp. 159–214.
41. J. W. Head and L. S. Crumpler, *Nature* **346**, 525 (1990).
42. P. Janle, D. Jannsen, A. T. Basilevsky, *Earth Moon Planets* **39**, 251 (1987).
43. E. R. Stofan and J. W. Head, *Icarus* **83**, 216 (1990).
44. A. A. Pronin and E. R. Stofan, *ibid.* **87**, 452 (1990).
45. Quetzalpetlatl has been proposed to the IAU as the name of this corona, but as of this writing the name has not been officially approved.
46. A. L. Sukhanov, *Geotectonics* **20**, 294 (1986).
47. D. L. Bindschadler and J. W. Head, *Icarus* 77, 3 (1989).
48. ———, *Earth Moon Planets* **42**, 133 (1988).
49. D. L. Bindschadler *et al.*, *Geophys. Res. Lett.* **17**, 171 (1990).
50. W. L. Sjogren *et al.*, *J. Geophys. Res.* **88**, 1119 (1983).
51. R. C. Kozak and G. G. Schaber, *Lunar Planet. Sci.* **17**, 44 (1986).
52. J. W. Head, *J. Geophys. Res.* **95**, 7119 (1990).
53. R. R. Herrick and R. J. Phillips, *Geophys. Res. Lett.* **17**, 2129 (1990).
54. D. L. Bindschadler and J. W. Head, *J. Geophys. Res.*, in press.
55. R. J. Phillips, R. E. Grimm, M. C. Malin, *Science*, in press.
56. R. White and D. McKenzie, *J. Geophys, Res.* **94**, 7685 (1989).
57. J. Weertman, *Phys. Earth Planet. Inter.* **19**, 197 (1979); D. L. Bindschadler and E. M. Parmentier, *J. Geophys. Res.* **95**, 21,329 (1990).
58. S. C. Solomon and J. W. Head, *Science* **252**, 252 (1991).
59. We are grateful to the engineering and mission support teams at the Jet Propulsion Laboratory, Martin-Marietta Corporation, and Hughes Aircraft Company whose dedicated efforts ensured the success of the Magellan mission. Important contributions to this work have been made by K. K. Beratan, D. L. Bindschadler, A. de Charon, S. L. Frank, P. G. Ford, D. M. Janes, L. Meinke, S. E. Smrekar, S. W. Squyres, and E. R. Stofan. R. E. Grimm, G. G. Schaber, R. A. Schultz, S. E. Smrekar, S. W. Squyres, and J. Suppe are thanked for helpful comments on earlier drafts. This research has been supported by NASA and by the U.K. Natural Environment Research Council.

14 January 1991; accepted 13 March 1991

Crystal Structure of Osmylated C_{60}: Confirmation of the Soccer Ball Framework

JOEL M. HAWKINS,* AXEL MEYER, TIMOTHY A. LEWIS, STEFAN LOREN, FREDERICK J. HOLLANDER

An x-ray crystal structure that confirms the soccer ball–shaped carbon framework of C_{60} (buckminsterfullerene) is reported. An osmyl unit was added to C_{60} in order to break its pseudospherical symmetry and give an ordered crystal. The crystal structure of this derivative, $C_{60}(OsO_4)$(4-*tert*-butylpyridine)$_2$, reveals atomic positions within the carbon cluster.

In 1985, KROTO, SMALLEY, AND CO-workers discovered that 60 carbon atoms form a particularly stable cluster in the gas phase. They proposed a simple and beautiful truncated icosahedral structure for C_{60} with a novel carbon framework resembling the seams of a soccer ball, and christened the molecule buckminsterfullerene (*1*). Late last year, Krätschmer, Huffman, and co-workers (*2*) reported that C_{60} could be prepared and isolated in macroscopic quantities (*3–5*). Since then, chemists and physicists have sought to confirm or disprove the soccer ball structure for C_{60}. The infrared (*2, 6*), Raman (*7*), ^{13}C NMR (*3, 8, 9*), and photoelectron spectra (*10*) are each consistent with icosahedral symmetry and are collectively highly supportive of the originally proposed structure, but they do not strictly prove the soccer ball framework or provide atomic positions. For example, the ^{13}C NMR spectrum (*8*) does not rule out the possibility of coincident peaks or a fluxional structure. We (*11*) and others (*2, 12*) have attempted to obtain a crystal structure of C_{60}, but could not determine specific atomic positions due to extensive disorder in the crystals. While the ball-like molecules pack in an ordered fashion, their nearly spherical symmetry promotes orientational disorder (*9*). We reasoned that if C_{60} could be derivatized in a way that broke its apparent spherical symmetry, it might crystallize with orientational order. We report here the synthesis of a one-to-one C_{60}–osmium tetroxide adduct and its crystal structure displaying the soccer ball framework of C_{60}.

Our recent report of the osmylation of C_{60} established that heteroatoms can be added to buckminsterfullerene without disrupting its carbon framework (*13*). Our conditions favored the addition of two osmyl units to C_{60}, giving the two-to-one adduct in 81% yield as a mixture of regioisomers (Scheme I). Chromatographic analysis of the crude reaction mixture revealed six peaks: five peaks corresponding to the precipitate which collectively analyzes with two-to-one stoichiometry, and a single sharp peak corresponding to toluene-soluble material. Use of one equivalent of OsO_4 increased the yield of the toluene-soluble material to 70%. Osmylation in the absence of pyridine, followed by dimer disruption with pyridine (*14*), gave the same species in 75% yield. The toluene-soluble material was shown to have one-to-one stoichiometry by converting it to the mixture of two-to-one adducts upon further exposure to the osmylation conditions. Solubility and crystal quality were improved by exchanging the pyridine ligands for 4-*tert*-butylpyridine.

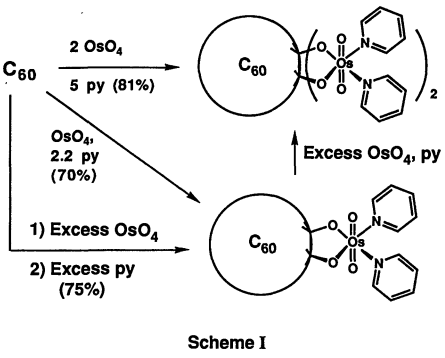

Scheme I

The observation of a single sharp chromatographic peak for the one-to-one adduct suggested that it is a single regioisomer, rather than a mixture of the two regioisomers which are possible from the proposed soccer ball structure for C_{60}. This would be

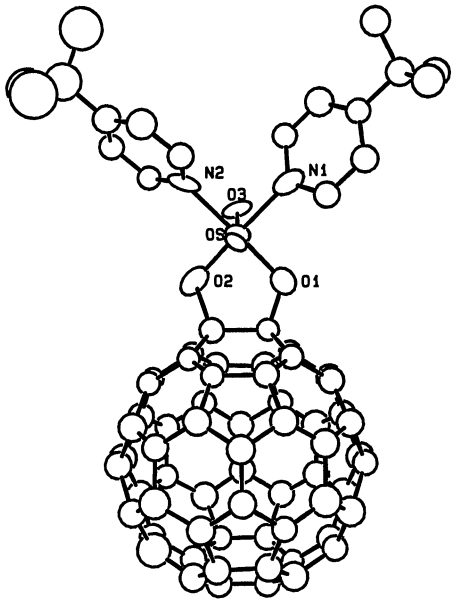

Fig. 1. ORTEP drawing (50% ellipsoids) of the one-to-one C_{60}–osmium tetroxide adduct $C_{60}(OsO_4)$(4-*tert*-butylpyridine)$_2$ showing the relationship of the osmyl unit with the carbon cluster.

Department of Chemistry, University of California, Berkeley, CA 94720.